Pergamon

Geochimica et Cosmochimica Acta, Vol. 67, No. 16, pp. 3079–3096, 2003

0016-7037/03 $30.00 + .00

doi:10.1016/S0016-7037(00)00306-5

Main-group pallasites: Chemical composition, relationship to IIIAB irons, and origin

JOHN T. WASSON[1,*] and BYEON-GAK CHOI[2]

[1]Institute of Geophysics and Planetary Physics, University of California, Los Angeles, CA 90095-1567, USA
[2]Department of Earth Science Education, Seoul National University, Seoul, 151-748, Korea

(*Received May* 30, 2002; *accepted in revised form April* 29, 2003)

Abstract—We used neutron activation to characterize the metal of 33 main-group pallasites (PMG), widely held to be samples of a core–mantle interface. Most PMG cluster in a narrow range of metal and silicate compositions, but 6 are assigned to an anomalous subset (PMG-am) because of their deviant metal compositions, and 4 others to another anomalous subset (PMG-as) because of their appreciably higher olivine Fa contents. Metal compositions in all PMG are closely related to those in evolved IIIAB irons, and are generally consistent with their formation in the IIIAB parent asteroid. On element-Au diagrams for incompatible elements the normal PMG plot near an extrapolation of IIIAB trends to higher Au concentrations. On element-Au plots of compatible elements such as Ir or Pt the loci of PMG spread out over a broader region explainable by mixing of evolved IIIAB magma with early-crystallized core or mantle-residue solids.

Two features of PMG require special models: (1) Ga and Ge contents are generally high (≈1.5×) compared to the IIIAB-based mixing model: and (2) the FeO/(FeO + MgO) ratios span a surprisingly wide range, from 0.11–0.14 in normal PMG to 0.16 to 0.18 in PMG-as This range is larger than expected in a cumulate layer at the base of a mantle. We suggest that both features may be related to the interaction of PMG precursors with a highly evolved magmatic gas phase, and that some or all of these anomalies may have resulted from vapor deposits in voids near the core–mantle interface.

An important boundary condition for understanding the detailed PMG origin at the core–mantle interface is the large difference between the solidus temperature of Fa11 olivine (≈2000 K) and the liquidus temperature of an evolved IIIAB melt containing >100 mg/g S and some P (≈1600 K). Following the mixing event that formed the PMG it is therefore reasonable that there would have been olivine rubble floating on top of the IIIAB-like magma, but with appreciable void space present just above the upper level reached by the magma. These voids would have contained gases released from the magma during its flow into the PMG region. We suggest that Ga and Ge, the two most volatile siderophiles in our element set, were added to PMG metal from the magmatic gas. We also suggest that the magmatic gas was oxidizing and that the PMG having high olivine fayalite contents formed in regions where the ratio of void to olivine was high, and that some metallic Fe was oxidized and entered the olivine (or the phosphoran olivine). In support of the latter idea is the observation that both Ni and Co are elevated in the PMG-as (Fa≥16) compared to values predicted by IIIAB trends.

We analyzed two Eagle-Station pallasites (PES); after correction for weathering effects in Cold Bay, its composition is found to closely resemble that of Eagle Station but to represent a more evolved composition (i.e., lower Ir, higher Au). Vermillion and Yamato 8451 have been called pyroxene pallasites but have metal compositions (unrelated to those of the PMG or PES) that are too different from each other to even allow assignment to the same grouplet.

1. INTRODUCTION

Pallasites are meteorites mainly consisting of Fe-Ni metal and olivine in subequal mass proportions. In some pallasites olivine is uncommon to rare; most specimens of Glorieta Mountain are olivine-free. There is confusion in the literature between the use of pallasite as a structural term and as a name (e.g., like "aubrite") used to designate a group of genetically related meteorites formed on the same parent body by the same or similar processes. Because the structural use of the term is pervasive, we recommend that the term pallasite used alone be confined to the structure, and that modifiers be added for groups or grouplets. We follow past practice (Davis, 1977; Scott, 1977a,b) and use main-group pallasite to describe the main compositional cluster, and Eagle-Station pallasites for the other, genetically distinct pallasite grouplet. The Eagle-Station pallasites differ from the main group in terms of O-isotope and metal compositions.

We propose to change the standard acronym abbreviations of pallasite groups. Wasson (1974) used PAL as the letter abbreviation for the main group, a usage now common in the literature. The problem with this is that it has the mnemonic implication that all objects with pallasitic structure belong to the same group. Some authors have used EST as the abbreviation for the Eagle-Station trio of pallasites, but this choice has the unfortunate consequence of having no mnemonic clue to the pallasitic structure, and the T would require replacement if one or more additional members are discovered. We therefore propose to use PMG as the new abbreviation for the main-group pallasites and PES for the Eagle-Station pallasites.

We report instrumental neutron-activation analysis for 33 PMG, two of the three PES, and two olivine-rich ungrouped irons, the so-called pyroxene-bearing pallasites, Yamato 8451 (Yanai and Kojima, 1995) and Vermillion (Boesenberg et al., 2000). The PMG are compositionally closely related to the

* Author to whom correspondence should be addressed (jtwasson@ucla.edu).

IIIAB irons (Scott and Wasson, 1976). One of the most important questions about the PMG is whether they originated in the same parent asteroid as the IIIAB irons. And, if the PMG are closely related to the high-Au, high-Ni extreme of the IIIAB group, how close is the compositional agreement and how is one to explain the observed differences?

2. STRUCTURE AND MINERALOGY

Pallasitic olivine can be either angular or round; the tabulation of Scott (1977b) shows the angular form to be present in 79% of recovered pallasites (Marburg, now paired with Brenham, was excluded from the statistics). There seems to be a generally accepted view that the typical median diameter ($\equiv$ (length $\times$ width)$^{1/2}$) of pallasitic olivine is greater than 4 mm; for example, Tucson, in which the median size of the dominant silicate, forsteritic olivine, is $\sim$2 mm, is never called a pallasite. With the possible exception of Vermillion, the stony-iron meteorites we discuss in this paper are structurally pallasites with coarse ($\geq$4 mm) olivine. Pallasitic olivine has been reviewed by Buseck and Goldstein (1969), Buseck (1977), Scott (1977b) and Davis (1977).

The major mineral assemblages of most PMG are quite simple, consisting of troilite and schreibersite in addition to olivine, kamacite and taenite; olivine Fa values range from 11 to 18 mol%, with $>$80% of the values in the range 11.6–13.5 mol% (Buseck and Goldstein, 1969). In addition, several characteristic minor minerals have been reported. Chromite is relatively abundant; some grains have euhedral shapes and seem to have crystallized from a melt (Buseck, 1977). A few chromites are quite massive; a large (10-cm) chromite-olivine assemblage in Brenham was reported by Francis and Lange (1987) and described in more detail by Wasson et al. (1999). Phosphates are minor phases in all PMG (common only in Springwater); the identified phosphates are farringtonite, $Ca_3(PO_4)_2$, stanfieldite, $Ca_4(Mg,Fe,Mn)_5(PO_4)_6$, and merrillite, $Ca_9(Mg,Fe)Na(PO_4)_7$ (Buseck and Holdsworth, 1977). Phosphoran olivine is rare in most pallasites but minor amounts may be ubiquitous in the more oxidized PMG (Buseck, 1977; Buseck and Clark, 1984). Low-Ca pyroxene is a rare accessory phase (Buseck, 1977), and a minor phase in the ungrouped pallasites Yamato 8451 and Vermillion.

The PES pallasites have mineral assemblages similar to PMG pallasites, but have different metal and olivine compositions (Buseck and Goldstein, 1969; Wasson, 1974). The mean Ni content of the metal is higher, and olivine Fa contents are slightly higher ($\approx$ Fa20) than those in the Zaisho (Fa18.3), which has the highest Fa among PMG (Buseck and Clark, 1984).

In the pyroxene-bearing pallasites Y8451 and Vermillion (Boesenberg et al., 1995; Yanai and Kojima, 1995) $\sim$5% of total silicates are pyroxenes.

3. SAMPLES AND ANALYTICAL TECHNIQUES

Mean elemental concentrations based on instrumental-neutron-activation-analysis (INAA) and radiochemical neutron-activation-analysis (RNAA) (for Ge and some Sb) data are listed in Table 1. Olivine compositions listed in Table 1 are mainly from Buseck and Goldstein (1969); because the mol% fayalite they report contains round-off errors; the listed values were recalculated from the wt% Fe and Mg. More recent olivine compositions reported by Smith et al. (1983) are in good to adequate agreement with these data. The O-isotopic compositions in Table 1 are mainly from Clayton and Mayeda (1996).

Our INAA procedures have evolved over the decades; the first UCLA INAA data on iron meteorites were obtained by E. Scott in 1973, and Scott analyzed numerous pallasites in 1973–74. In 1979 we augmented the INAA data set to include Cu and Pt, began using Fe as a control of sample shape, and instituted corrections for γ-ray self absorption. In 1986 we went to a uniform sample thickness that eliminated the need for self-absorption corrections and used Fe as an internal standard of counting geometry and, to a lesser extent, the presence of nonmetallic phases. In our present procedure our primary standard for most elements is the Filomena IIAB specimen of the North Chile hexahedrite, with NBS steel 809b used as the primary Cr, Sb and As standard and as a secondary standard for a few other elements. We now also include the IIAB Coahuila iron as a third standard, especially for Re and Pt.

The preparation for INAA of pallasitic samples differs by only a minor degree from the iron-meteorite protocol outlined in Wasson et al. (1989) and Wasson and Kallemeyn (2002). In samples containing appreciable olivine the metal is commonly cut into two 1.5-mm thick slices (rather than a single 3 mm slice) to allow more thorough removal of the olivine. Two slices having a total mass in the range 450–650 mg are stacked to produce our standard 3-mm counting thickness. About 30% of our samples were from metal veins completely or nearly olivine free and were analyzed as 3-mm-thick pieces. With a few exceptions the pallasites were analyzed two or more times.

As discussed by Davis (1977), sampling pallasite metal presents more serious problems than encountered with irons including even the closely-related, schreibersite-rich high-Ni IIIAB irons. Pallasite metal samples often contain appreciable ($>$3%) amounts of olivine or chromite; our corrections for these are only approximate but minor. More serious, elemental concentrations in pallasite metal are strongly impacted by sampling errors in the kamacite/taenite ratio. Kamacite "swathes" the olivine, an indication that kamacite nucleated on the olivine, and depending on the amount of Ni diffusion through the parental taenite, can lead to enhancements of the kamacite/taenite (k/t) ratio in olivine-rich samples. As discussed below, our analyses of Brenham suggest that samples from olivine-rich regions have higher k/t ratios than those from metal-rich "vein" regions.

Swathing kamacite tends to be selectively ground off by the mechanical abrasion used to remove olivine. It is also a common neutron-activation procedure to clean surfaces by light etching after irradiation, and the high surface-to-mass ratios of pallasite metal samples combined with the higher etch rate of kamacite compared to taenite inevitably leads to a decrease in the k/t ratio in the counted sample. We minimized the latter problem by reducing the etching durations of our pallasite samples relative to the iron meteorites, and some high-surface-area samples were not subjected to this acid cleaning.

Cobalt is the element most affected by nonrepresentative sampling of kamacite, made prominent because of our high precision for this element and its small total range. At low temperatures the k/t equilibrium ratio of Co is $\sim$5 (Sears and Axon, 1976; Afiattalab and Wasson, 1980). In more than half our PMG metal analyses Co values plot lower than the IIIAB Co-Au trend. The only element other than Co that we know to have a k/t concentration ratio $>$1 is As (Davis, 1977); we do not know the equilibrium k/t ratio at diffusional blocking temperatures around 400–500 K.

In some pallasites selective corrosion of kamacite has occurred; PES Cold Bay is a key example. Even in the least weathered Cold Bay samples only the taenite and the thick, primary kamacite has survived; fine kamacite originally present in plessite is replaced by iron oxide. During the replacement process it is inevitable that some of the elements from the oxidized kamacite escape from the system and are not included in the analysis. We assumed that the difference between 990 mg/g and the sum of Fe and Ni was the maximum weight fraction of kamacite that had been replaced by O during oxidation; to avoid overcorrection of Fe and Co we only added an amount of kamacite equal to half the apparent amount of O. Relative to the other siderophiles we increased Fe by $\sim$14% and Co by $\sim$28% in our INAA runs. The main uncertainty is associated with the Co correction.

Many pallasite samples contained appreciable amounts of chromite leading to elevated Cr contents and slightly lower contents of other elements. Our policy is to include these Cr data in the average. Even the

Table 1. Mean concentrations of 13 elements in 33 PMG, 2 PES and 2 olivine-rich ungrouped irons (IrUn). Concentrations in μg/g except Co and Ni (mg/g) and Sb and Re (ng/g). Italic samples are paired with other pallasites on the list.

Meteorite	cls	an?	Cr	Co	Ni	Cu	Ga	Ge	As	Sb	W	Re	Ir	Pt	Au	oliv[a]	$\Delta^{17}O$[a]
Acomita	PMG		4910	5.62	130.2	300	18.0	55.1	24.7	218	0.23	<40	0.030	3.6	2.733	12.0	
Admire	PMG		650	5.33	117.6	249	21.3	43.8	24.6	340	0.24	<40	0.019	1.2	2.910	12.1	−0.32
Ahumada	PMG		1480	5.24	93.6	143	20.9	49.0	19.5	380	0.39	<34	0.057		2.226	11.6	−0.27
Albin	PMG		336	5.36	108.4	212	17.1	29.4	21.7	<250	0.18	<50	0.017	5.7	2.771	11.6	−0.30
Barcis	PMG		12	5.39	104.8	187	21.1	<60	26.9	<200	0.51	24	0.316	1.9	2.742	11.6	
Brahin	PMG		3920	5.51	111.6	185	24.3	60.7	25.7	185	0.30	<30	0.107	2.2	3.021	11.7	−0.31
Dora (pal)	PMG		1750	5.34	115.5	251	17.1	33.4	20.3	280	0.29	<20	0.100	1.8	2.531	12.9	−0.15
Esquel	PMG		224	5.21	93.1	121	23.0	55.5	18.0	<200	0.25	<50	0.022	1.6	2.050	11.7	−0.25
Finmarken	PMG		60.0	5.70	102.8	165	18.8	43.7	27.7		0.28	278	2.08	4.8	2.545	12.7	−0.24
Giroux	PMG		36	4.83	106.7	170	23.2	49.2	17.1	155	0.27	<30	0.023	1.4	2.138	10.8	
Ilimaes (pal)	PMG		15	5.39	102.9	165	21.0	44.7	23.6	290	0.24	<20	0.131	4.2	2.601		−0.34
Imilac	PMG		64	5.85	82.8	149	20.9	47.7	27.0		0.25	<30	0.090	2.3	2.247	12.3	−0.27
Lipovsky	PMG		60	5.29	109.6	225	18.2	30.8	24.1	325	1.58	<50	0.09		2.698	11.6	−0.40
Marjalahti	PMG		6400	5.60	87.5	111	22.9	54.7	18.5	<220	0.28	268	2.13	4.7	1.842	11.9	−0.29
Molong	PMG		14	5.60	99.9	139	21.2	61.2	22.5	217	0.24	22	0.208	3.7	2.545	11.3	−0.26
Mount Vernon	PMG		2550	5.73	109.1	267	21.3	49.1	27.0	148	0.41	14	0.144	3.4	2.508	11.9	
Newport	PMG		17	5.32	115	249	17.5	31.2	25.9	<200	0.21	<40	0.17	<2.8	2.570	11.8	
Omolon	PMG		997	5.79	89.2	151	19.5	<60	26.4	<200	0.14	<20	0.023	1.5	2.417	12.2	
Otinapa	PMG		54	5.18	108.6	172	18.2	36.4	24.2	222	0.33	<30	0.227	3.2	2.569	13.0	−0.29
Pecora Es PCA91004	PMG		32	5.12	95.7	128	23.7	57.4	15.8	166	0.33	78	0.764	3.0	2.006	11.2	
Quijinque	PMG		210	5.27	101.0	153	20.6	<60	21.4	<240	0.12	<20	0.058	2.1	2.368		
South Bend	PMG		330	5.38	92.2	145	20.8	44.5	20.0	99	0.19	<25	0.058	1.6	2.194	12.0	−0.22
Thiel Mountains	PMG		43	5.72	97.4	126	22.0	50.2	25.1		0.27	<50	0.209		2.670	12.6	
Yamato Y74044	PMG		934	5.40	91.6	162	19.1	42.9	24.4	317	<.4	<50	0.017		2.671	11.9	
Argonia	PMG	AM	80	5.60	123.6	202	18.7	37.3	24.7	235	0.37	710	6.52		2.770	13.5	
Brenham (Marburg)	PMG	AM	<20	5.28	117.3	177	25.9	70.6	23.2	321	0.38	<70	0.026	3.7	2.733	12.5	
Brenham metal vein	PMG	AM	15	5.62	104.6	173	25.0	67.5	24.9	170	0.24	<40	0.027	4.0	2.648		
Brenham pal struct	PMG	AM	16	5.17	107.6	203	25.8	67.5	22.1	280	0.33	<40	0.039	4.9	2.764	12.4	−0.32
Glorieta Mountain	PMG	AM	14	5.63	116.7	272	14.0	10.7	25.0	282	0.19	<40	0.014	<3.5	2.818	13.2	−0.31
Huckitta	PMG	AM	1850	5.20	85.0	108	27.0	65.4	17.1	230	0.56	100	0.988	6.2	1.724	12.7	
Krasnojarsk	PMG	AM	25	6.31	83.0	105	20.9	55.9	31.4	393	0.55	<40	0.215	2.8	2.414	12.2	−0.41
Pavlodar	PMG	AM	280	5.01	82.0	125	24.0	74.0	9.58	<150	0.87	600	5.15	10.7	1.132	12.7	
Phillips County h-Ir	PMG	AS	1720	5.17	136.0	253	18.3	35.0	27.2	430	0.24	360	3.33	1.8	4.03		
Phillips County l-Ir	PMG	AS	20	6.35	132.1	155	15.5	34.4	22.7	<200	0.13	<50	0.085	2.8	2.813	17.9	
Rawlinna (pal)	PMG	AS	39	6.10	135.3	256	18.2	43.0	24.6		0.15	<50	0.069	3.5	2.297	15.9	
Springwater	PMG	AS	26	5.88	121.8	137	15.5	31.9	26.4	<230	0.31	<40	0.076	1.7	2.910	17.9	−0.27
Zaisho	PMG	AS	186	5.91	104.3	239	14.7	23.9	24.5	350	0.27	<50	0.041	<2.7	2.629	19.0	
Cold Bay[b]	PES		1160	8.90	206.0	441	9.05	113	9.44	230	0.26	735	8.56	20.0	1.224	19.3	
Eagle Station	PES		9410	8.64	153.1	416	5.25	75.0	10.7	345	0.50	1240	12.8	22.0	0.970	20.0	−4.51
Vermillion	IrUn		41	4.88	74.9	122	46.2	147	12.9	124	0.59	237	1.96	2.0	1.415	11.9	−0.76
Yamato 8451	IrUn		90	7.98	145.4	522	19.6	59	19.4	1169	1.49	738	6.87	16.6	2.102	10.6	−0.77

[a] Olivine composition in units of %Fa (Buseck and Goldstein, 1969; the listed values were recalculated from the wt% Fe and Mg that they report); $\Delta^{17}O$ units are ‰, from Clayton and Mayeda (1996).
[b] Cold Bay values include corrections for kamacite lost during weathering; see text.

lowest Cr contents in Table 1 should be taken as upper limits of the Cr content of metal phases. In addition, Wasson and Richardson (2001) noted that there is an elemental interference by Fe that causes our Cr values to be high by roughly 6 μg/g. Our Cr data are not corrected for this interference.

Mean INAA concentrations of twelve elements and RNAA concentrations for Ge in pallasites and related meteorites are listed in Table 1. Because pallasite metal tends to show considerable scatter we list our replicate data in Table 2; older (before 1986) or less precise INAA data were assigned less weight in calculating means. Older data have been reevaluated to correct for small (generally a few percent or less) calibration errors. No INAA Ge replicates are reported in this paper; the mean values listed in Table 1 are based on RNAA data. Most have been previously published by Wasson and Sedwick (1969), Wasson (1974), Scott (1977a), and other UCLA papers.

In the 1970s our INAA technique sometimes produced a high scatter for Ni replicates, and for Ir data at concentrations <0.1 μg/g; during this period our atomic-absorption Ni and, at low concentrations, our RNAA Ir values were superior. During the last two decades the quality of INAA Ni data is equal to that of atomic absorption. In the reported means the published atomic-absorption Ni data are treated as one additional replicate. Most of the mean Ir data in Table 1 are based on INAA data. With one or two exceptions, all PMG Sb values are high enough to determine at ~10% precision by INAA, but most of the IIIAB data plotted in a later diagram are RNAA values from Willis (1980) and unpublished.

The relative sample standard deviation of our INAA technique based on 13 analyses of a specimen of Canyon Diablo (with the high inclusion content typical of IAB metal) is 2% for Co, Au, and Ni, 3–5% for Ga, As and Ir, 6–9% for Cu, Pt and W, and 11% for Sb and Re (Wasson and Ouyang, 1990). Because of stochastic variation in the Cr content it is not possible to determine a meaningful standard deviation for Cr. Standard deviations are somewhat higher for concentrations below 0.3 μg/g W; 200 ng/g Re, 0.1 μg/g Ir, and 2 μg/g Pt.

4. RESULTS AND CLASSIFICATION

4.1. O-Isotopic Composition of Pallasites

We discuss the O-isotope data (Fig. 1, data from Clayton and Mayeda, 1996) before the elemental data because the former

Table 2. Individual analyses of pallasites carried out during 1986 or more recently. Concentrations in μg/g except Co and Ni (mg/g) and Sb and Re (ng/g).

Meteorite	Yr	Mo	Cr	Co	Ni	Cu	Ga	As	Sb	W	Re	Ir	Pt	Au
Acomita	93	7	9646	5.73	126.3	270	18.2	25.2	240	0.31	<52	0.032	3.7	2.764
Acomita	93	9	174	5.51	134.1	329	17.8	24.1	166	0.19	<46	0.028	3.5	2.702
Admire	96	4	1270	5.23	128.4	252	20.6	24.4	330	0.20	<50	0.023	1.0	2.901
Admire	96	5	35	5.37	120.6	247	19.7	23.3	360	0.21	<40	0.016	1.4	2.865
Ahumada	93	2	2590	5.21	96.2	148	21.7	20.0		0.44	<37	0.059	2.1	2.190
Ahumada	93	7	373	5.26	98.0	138	19.7	19.0	380	0.34	<34	0.054	2.4	2.262
Albin	97	3	10	5.49	107.4	210	17.1	21.1	<250	0.18	<50	0.018	5.7	2.801
Barcis	97	7	14	5.31	104.0	188	21.0	26.6	<200	0.93	24	0.318	1.7	2.817
Barcis	97	11	10	5.47	105.6	187	21.2	27.1	230	0.09	<30	0.314	2.1	2.666
Brahin	96	1	7056	5.86	130.2	185	24.4	25.8	<190	0.43	<73	0.125	<2.5	3.025
Brahin	95	11	784	5.16	112.5	185	24.1	25.6	185	0.22	<30	0.107	1.7	3.017
Brahin	95	11	3700	5.27	96.0	149	26.3	25.6	101	0.27	<44	0.126	3.7	2.593
Brenham (Marburg)	96	1	36	5.38	101.9	169	25.0	24.3	340	0.33	<70	0.037	3.7	2.752
Brenham metal vein	96	1	15	5.74	98.2	169	25.4	26.1	150	0.26	<67	0.027	4.0	2.649
Brenham metal vein	96	5	14	5.50	107.8	178	24.7	23.7	190	0.23	<40	0.027	3.9	2.647
Brenham pal struct	96	1	16	5.15	107.7	206	25.0	20.4	180	0.29	<64	0.037	5.0	2.767
Brenham pal struct	96	5	16	5.18	107.5	200	26.7	23.7	380	0.38	<40	0.041	4.8	2.760
Cold Bay[a]	96	1	2231	8.86	206.8	425	8.80	9.39	170	0.28	840	8.67	20.0	1.252
Cold Bay[a]	96	5	95	8.94	205.1	457	9.30	9.48	290	0.23	630	8.44	19.9	1.195
Dora	93	2	283	5.27	119.6	277	17.8	20.7		0.30	<20	0.096	1.5	2.520
Dora	93	7	3220	5.42	111.4	224	16.3	19.9	280	0.29	<26	0.104	2.0	2.541
Eagle Station	96	1	9977	8.48	149.6	414	5.10	10.5	340	0.61	1380	12.6	20.4	0.952
Eagle Station	96	5	8838	8.80	155.7	418	5.40	10.9	350	0.39	1090	13.0	23.6	0.987
Esquel	97	3	9	5.23	91.4	124	23.2	18.7	<250	0.20	<140	0.022	2.9	2.043
Esquel	96	5	648	4.94	103.1	131	22.3	16.8	180	0.16	<50	0.025	1.5	2.130
Esquel	96	10	14	5.45	86.5	107	23.5	18.5	<200	0.39	<130	0.020	1.1	1.978
Finmarken	93	2	19	5.73	101.0	165	18.1	26.9		0.28	275	2.01	5.2	2.440
Finmarken	93	2	100	5.67	100.5	164	19.6	28.5			281	2.15	4.3	2.650
Giroux	02	6	43	4.99	102.8	146	23.2	17.6	<160	0.22	<40	0.023	1.6	2.074
Giroux	02	10	29	4.67	110.5	194	23.5	16.5	155	0.16	<30	0.022	1.3	2.202
Glorieta Mtn	93	9	14	5.64	117.5	304	15.4	23.2	229	0.20	<40	0.019	<3.5	2.698
Glorieta Mtn	91	3	14	5.59	116.6	233	13.6	26.0		0.16	<45	0.009	<3.4	2.770
Glorieta Mtn	91	4	14	5.76	116.0	291	14.8	26.3	335	0.20	<45		3.6	2.970
Huckitta	97	3	2100	5.21	85.4	110	27.2	17.6	230	0.58	110	0.980	6.3	1.752
Huckitta	93	2	1601	5.20	91.7	105	27.9	16.6		0.53	91	0.996	6.1	1.697
Imilac	97	7	12	5.36	101.3	156	21.6	25.5	270	0.24	<13	0.130	2.0	2.584
Imilac	95	11	107	5.85	75.3	177	19.9	26.9		0.30	<30	0.084	2.2	2.144
Imilac	93	2	21	5.85	82.0	121	22.1	27.1		0.20	<40	0.096	2.4	2.350
Imilac	93	9	12	5.36	105.8	167	21.4	23.1	310	0.19	<50	0.136	6.2	2.571
Imilac	91	4	21	5.44	100.5	173	20.8	22.1	<370	0.28	<50	0.127	4.3	2.648
Krasnojarsk	96	4	12	6.64	67.6	83	20.3	33.6	500	0.54	<50	0.222	4.5	2.311
Krasnojarsk	96	5	32	6.15	84.8	116	21.2	30.6	340	0.56	<40	0.212	1.9	2.465
Marjalahti	96	1	1251	5.48	88.1	123	22.6	17.3	250	0.20	285	2.16	6.0	1.954
Marjalahti	95	11	286	5.72	86.8	99	23.1	20.7	<220	0.36	250	2.11	3.3	1.729
Molong	97	11	11	5.45	104.5	149	20.7	20.6	234	0.22	22	0.204	4.1	2.637
Molong	97	9	16	5.76	95.2	128	20.9	24.4	199	0.25	23	0.211	3.2	2.452
Mount Vernon	02	6	3112	5.84	100.3	264	20.8	27.5	118	<0.5	<22	0.147	3.3	2.457
Mount Vernon	02	10	1983	5.61	112.0	269	21.5	26.4	177	0.30	14	0.140	3.5	2.558
Newport	97	3	14	5.24	116.2	275	18.1	25.2	240	0.21	<40	0.174	4.2	2.721
Newport	97	7	19	5.39	114.6	223	16.9	26.5	<200	0.22	1.4	0.163	<1.5	2.419
Omolon	99	3	1290	5.93	84.1	146	19.5	27.8	165	0.21	<20	0.020	1.6	2.336
Omolon	99	4	703	5.64	94.3	155	19.4	25.0	<200	0.09	<40	0.026	1.5	2.497
Otinapa	86	8	75	5.32	103.3	162	21.5	27.6	304	0.57	<26	0.251	4.5	2.591
Otinapa	86	11	33	5.04	113.8	182	18.3	20.9	254	0.17	<30	0.203	1.9	2.547
Pavlodar	96	1	399	5.23	74.1	109	22.8	9.58	<200	0.89	626	5.01	10.5	1.069
Pavlodar	95	11	161	4.79	92.7	140	25.2	9.58	<150	0.85	575	5.29	10.9	1.194
Pecora Es PCA 91004	93	2	28	5.04	97.2	134	24.3	16.2		0.32	91	0.782	2.2	2.010
Pecora Es PCA 91004	93	7	36	5.19	94.1	122	23.0	15.4		0.33	65	0.746	3.7	2.001
Phillips County h-Ir	96	1	1725	5.17	136.0	253	18.3	27.2	430	0.24	362	3.33	1.8	4.027
Phillips County l-Ir	96	5	20	6.35	132.1	155	15.5	22.7	<200	0.13	<240	0.085	2.8	2.813
Quijinque	99	3	409	5.12	106.9	171	21.7	20.3	235	0.13	<20	0.060	2.3	2.451
Quijinque	99	4	11	5.41	95.0	134	19.4	22.5	<200	0.12	<40	0.056	1.9	2.285
Rawlinna (pal)	96	1	56	6.01	132.2	254	17.5	23.7		0.16	<74	0.069	1.0	2.281
Rawlinna (pal)	96	4	22	5.98	138.3	257	18.4	25.5	<200	0.13	<50	0.069	5.9	2.312
South Bend	99	3	38	5.38	91.6	143	21.3	21.0	77	0.130	<24	0.057	1.5	2.248
South Bend	99	5	622	5.37	91.3	147	20.0	19.0	120	0.260	<25	0.059	1.7	2.139
Springwater	96	1	39	6.19	108.3	134	15.2	28.6	<230	0.20	<40	0.087	1.2	2.767
Springwater	93	7	14	5.57	131.1	140	15.7	24.2		0.48	<51	0.065	2.3	3.052
Vermilion	95	3	61	4.89	73.5	123	44.4	12.5		0.57	240	1.90	<2.0	1.383
Vermilion	95	11	20	4.86	76.4	121	47.9	13.3	<200	0.60	234	2.02	3.3	1.446
Yamato 8451	96	1	148	8.16	140.2	521	19.2	19.4	1190	1.50	736	6.96	19.7	2.145
Yamato 8451	95	11	31.1	7.79	150.6	523	19.9	19.4		1.47	739	6.78	13.4	2.059
Zaisho	96	4	17	5.72	120.1	274	14.4	22.4	410	0.27	<240	0.044	<2.7	2.794

[a] Cold Bay values include corrections for kamacite lost during weathering; see text.

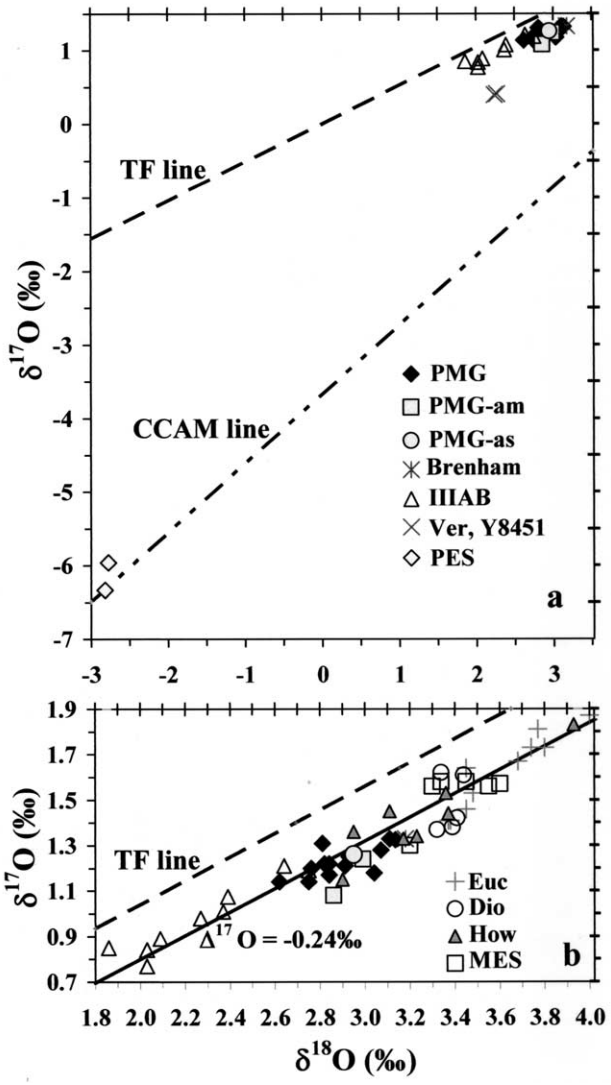

Fig. 1. Oxygen isotopic compositions of pallasites and related meteorites. (a) Meteorites having pallasitic structures form (1) one large group (main-group pallasites or PMG) plotting with the HED meteorites and IIIAB irons 0.2‰ below the terrestrial fractionation line; (2) a cluster of PES plotting 4.6‰ below the TF line; and (3) two other so-called pyroxene pallasites that form a cluster 0.8‰ below the TF line. These large differences imply formation of the parent bodies at widely separated locations and/or times, and thus indicate assignment to different clans. (b) A detailed comparison of O-isotopic compositions in PMG with closely related IIIAB irons, HED achondrites and mesosiderites shows that all have $\Delta^{17}O$ relatively close to -0.2‰, with the mean PMG composition (about -0.29‰) somewhat lower than the means for the other sets. Data mainly from Clayton and Mayeda (1996).

offer indisputable evidence that the main-group pallasites (PMG) and Eagle-Station pallasites (PES) must be separated into different clans. In Figure 1a we compare the PMG olivines with those from PES and the ungrouped olivine-rich meteorites Vermillion and Yamato 8451. The mean PMG $\Delta^{17}O$ ($=\delta^{17}O - 0.52 \cdot \delta^{18}O$) value is -0.28 ± 0.06‰ (error is 1σ). The mean PES $\Delta^{17}O$ value is much lower, ≈ -4.6‰. Yamato 8451 and Vermillion plot intermediate between PMG and PES pallasites and have similar O-isotope compositions ($\Delta^{17}O \approx -0.76$‰); their $\Delta^{17}O$ values show that these are not related to either the PMG or the PES. As discussed by Boesenberg et al. (2000) and Wasson and Kallemeyn (2002), our INAA metal data for Vermillion and Y8451 show that they are also not closely related to each other.

Figure 1b shows the relationship between the PMG pallasites, the HED meteorites, the mesosiderites and the chromite, phosphates and one silicate from IIIAB irons. The data in Figure 1b suggest that the mean $\Delta^{17}O$ of the PMG is 0.09% more negative than that of the IIIAB oxide phases; to show this we have drawn a reference fractionation line at $\Delta^{17}O \approx -0.24$‰; most IIIAB data plot above, most PMG data below this line. If we take these results at face value, a Student's *t*-test indicates that the PMG and IIIAB mean $\Delta^{17}O$ values are significantly different at a >99% confidence level.

This difference is of great potential importance. However, minor contamination of a few samples could also produce systematically lower (or higher) values. The first analysis of one pallasite, Brahin ($\Delta^{17}O = -0.31$‰) was originally reported to be -0.89‰.

Also plotted on Figure 1b are data for the closely related HED achondrites and the mesosiderites. The mean $\Delta^{17}O$ values in these groups are intermediate between those in the PMG and IIIAB but somewhat closer to PMG. It seems clear that a new investigation of the PMG and the IIIAB oxide phases is required to resolve any differences in $\Delta^{17}O$ among these meteorites.

At the high temperatures at which pallasites formed, chromite is expected to have $\delta^{18}O \sim 1$‰ lower than that of olivine in isotopic equilibrium. In fact, one chromite datum from the Brenham pallasite falls within the range reported for IIIAB chromite (Clayton and Mayeda, 1996).

4.2. Elemental Compositional Relationships among Pallasites and IIIAB Irons

The close relationship between PMG and IIIAB has been recognized since the first PMG metal analyses were published by Wasson and Kimberlin (1967). And the idea that pallasites are samples of a core–mantle boundary is much older still.

Because of the importance of the potential relationships between PMG and the IIIAB irons we show data for both sets of meteorites on most diagrams. Some of the IIIAB data were published by Wasson (1999a). The remaining data will be submitted for publication in the near future. To reduce clutter we do not plot the PES or the so-called pyroxene pallasites on these diagrams. We follow past practice for the iron meteorites and pallasites and plot all elemental data on logarithmic axes, and our recent practice (e.g., Wasson, 1999a) of using Au rather than Ni as the independent variable. That Au is the better independent variable results from the experimental (including sampling) scatter in Ni and Au being similar, but the range in Au being much larger. As a result, the Au concentration provides a much better estimate of a meteorite's position within the IIIAB fractional crystallization sequence, and, according to Wasson (1999a), its relative content of trapped melt.

In Figures 2 and 3, we show IIIAB and PMG data plotted on 10 element-Au diagrams. On most diagrams the position of the PMG is consistent with them being very evolved members of

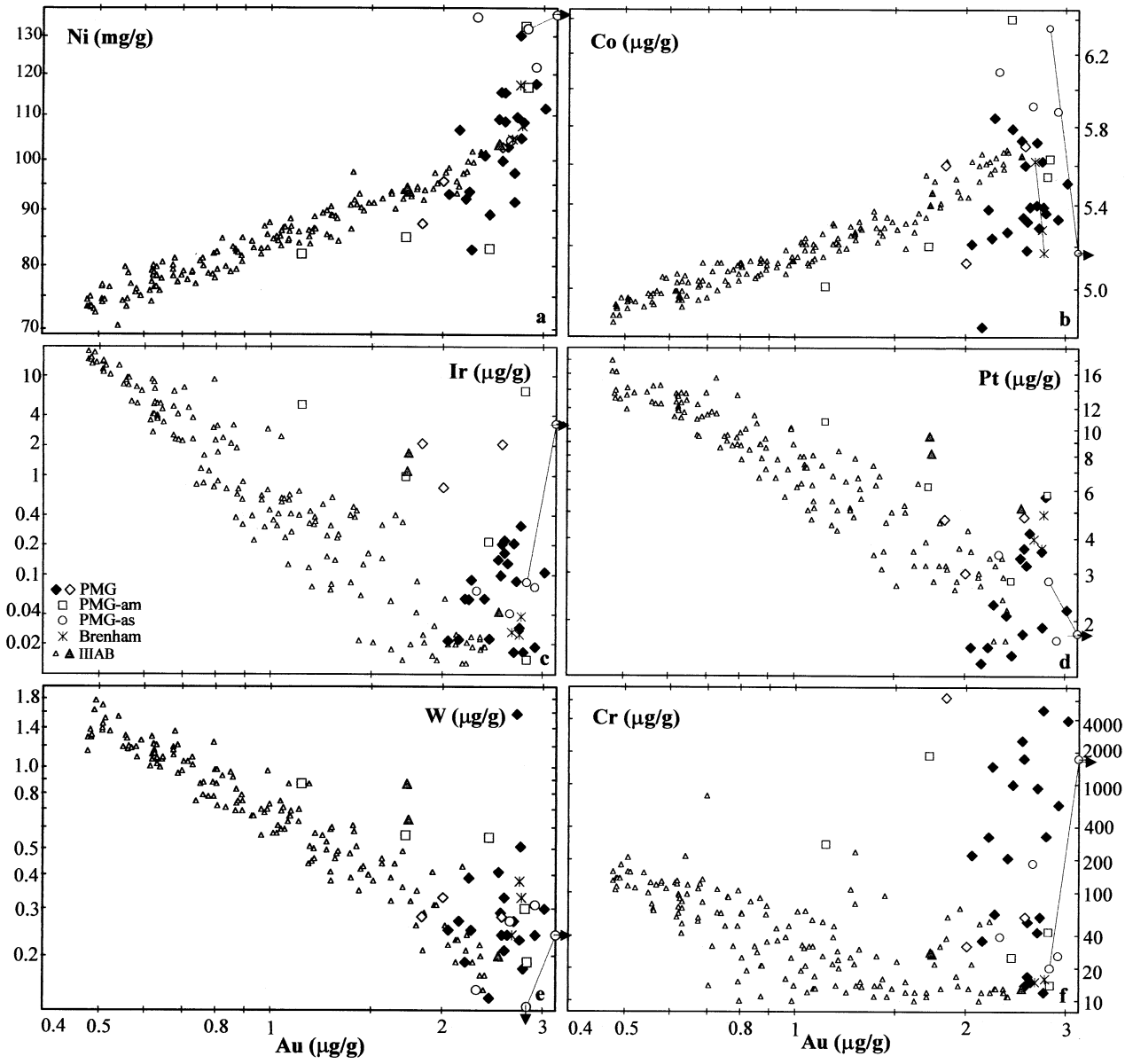

Fig. 2. Element-Au distributions for Ni, Co, Ir, Pt, W and Cr in metal samples from the main-group pallasites (PMG) are plotted together with data for IIIAB irons. Solid and liquid fractionation tracks for IIIAB are essentially the same as those in Wasson (1999a). Normal PMG are shown by dark and light diamonds; 10 anomalous PMG are shown with separate symbols. Most PMG plot near the high-Au extreme of IIIAB, generally consistent with past interpretations that they may have formed at the core–mantle interface of the IIIAB parent asteroid. Points connected by lines are data for separate samples of the same PMG; one Au value of 4.0 μm/g (for Phillips County) is plotted (with an arrow attached) at 3.2 μg/g. Three IIIAB irons shown with larger, shaded symbols fall outside the area bounded by solid and liquid tracks.

IIIAB, but there is much scatter about the IIIAB trend and some of the PMG fields clearly require more complex explanations.

We list ten PMG as anomalous and assign them separate symbols. Six that have metal compositions very different from most main group members are designated PMG-am (anomalous metal); one of these, Brenham, is given a unique symbol because it is necessary to discuss the differences between three different samples. Four PMG having fayalite contents much higher than those in most PMG are designated PMG-as (anomalous silicates). For convenience in later discussions we also represent three "unusual" PMG having moderately high Ir contents with the same symbols used for normal PMG but different shading. Because the paired samples Imilac and Ilimaes differ in composition, their points are connected on some diagrams, as are the very different Phillips County replicates (one of which contains 4 μg/g Au, and plotted on the axis at 3.1 μg/g with an arrow indicating that it is off scale).

In Figure 2 are element-Au diagrams for Ni, Co, Cr, Pt, W and Ir. Nickel (Fig. 2a) shows a much larger range than is observed in the adjacent part of IIIAB. Most of the Ni scatter

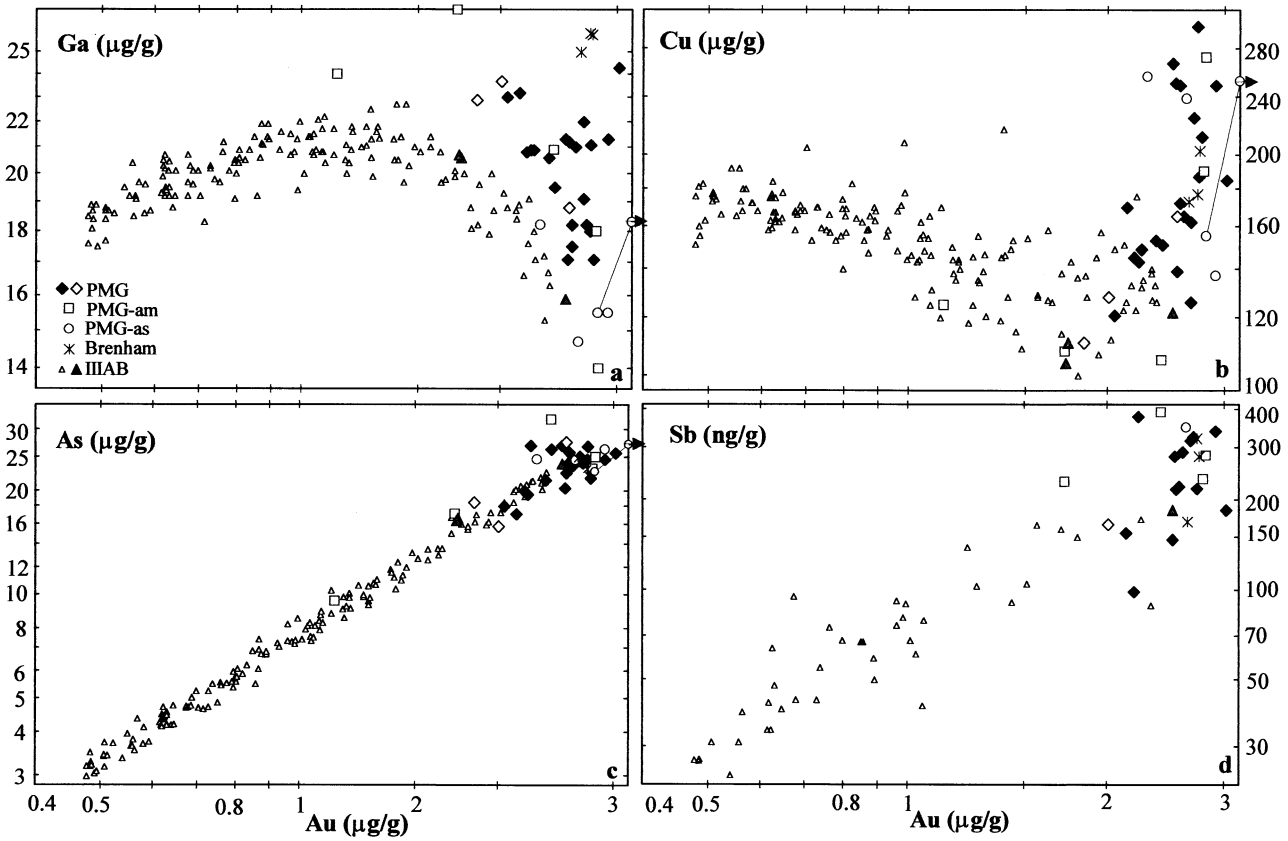

Fig. 3. Element-Au distributions for Ga, Cu, As and Sb in metal samples from the main-group pallasites (PMG) are plotted together with data for IIIAB irons. The PMG cluster near the high-Au extreme of IIIAB on the Sb-Au diagram, but relationships are more complex in the other two sets. With the exception of three anomalous PMG, all PMG Ga values plot above or right of the crescent shaped IIIAB trend. The IIIAB trend is initially negative but later flat; the PMG Cu-Au data scatter about a positive trend extending upwards from the high-Au extreme of this trend. PMG Co values range from below to above the IIIAB trend, apparently because of unrepresentative sampling of kamacite/taenite ratios; Imilac and Phillips County samples fall on both sides, Brenham samples plot below and within the IIIAB trend.

variations in the kamacite/taenite (k/t) ratio. Deletion of all low Co (=high kamacite) PMG would leave only Acomita appreciably above the IIIAB Ni-Au trend. The Co-Au diagram (Fig. 2b) shows a positive trend with low slope through group IIIAB. Almost all IIIAB irons plot within 2% (±0.1 mg/g) of the trend. A small set of 7 PMG, 2 PMG-am, 2 PMG-as and the Brenham metal vein sample fall within ± 0.25 mg/g of an extension of the IIIAB Co trend to higher Au contents. Three samples (1 PMG-am, 2 PMG-as) plot above the trend, and 13 PMG, one PMG-am and two Brenham samples (including Marburg) with pallasitic structures plot below the trend. Note that the points representing separate samples of Brenham and Imilac are connected, and that one of each set plots on or just above the IIIAB trend, the others below the trend.

On the Ir-Au diagram (Fig. 2c) only two PMG, Giroux and Esquel, plot within the IIIAB field; three anomalous IIIAB (Treysa, Delegate, Tieraco Creek—shown with larger shaded triangles) are outside from the IIIAB bounding curves. Scott (1977c) noted that the field populated by the PMG could be explained by mixing of a late (evolved) IIIAB melt with an early solid. We will discuss this model in more detail in a later section. Note that the three low-Au, high-Ir PMG shown with different shading plot near the anomalous IIIAB Delegate and Treysa.

The relative positions of PMG and IIIAB on the Pt-Au (Fig. 2d) and W-Au (Fig. 2e) diagrams are similar to those on the Ir-Au diagram Ir; like Ir, Pt and W are refractory but the latter two elements show much lower degrees of fractionation. Not plotted, the refractory and compatible siderophile Re shows fractionations similar to Ir but is near or below our detection limit in most PMG.

The IIIAB trend for Cr (Fig. 2f) is superficially similar to those of Pt and W. There is a major difference, however, in that Cr values in PMG are far too high to allow formation by a mixing model involving a melt composition on the lower right part of the diagram. Wasson et al. (1999) carried out a detailed study of a Brenham sample containing massive chromite replacing the metal in the pallasite structure, and argued that the negative Cr-Au trend observed in low-Au (≤1 μg/g) IIIAB irons is a sampling artifact, and that the solid-liquid distribution ratio is less than unity, probably near the value of 0.5 measured in laboratory experiments. According to this picture the very high Cr values commonly observed in PMG are a reflection of the high amount of Cr present in the highly evolved magma and

the fact that the pallasite structure makes it more difficult to avoid small chromites when choosing metal samples for analyses. An ironic observation consistent with this view is that our Brenham metal samples were relatively free of chromite, perhaps in part because ripening or the massive chromite reduced the content of tiny chromites adjacent to or enclosed in the metal. Note that Brenham's rounded olivine also indicates a greater amount of metamorphic elemental transport than occurred in the pallasites with angular olivine.

In Figure 3 we show element-Au distributions for Ga, Cu, As and Sb. The Ga-Au IIIAB trend (Fig. 3a) shows the well-know crescent shape. Later in the paper we model this with a Ga solid/liquid distribution ratio D_{Ga} that rises from ~0.97 at the onset of crystallization to 2.2 at 80% crystallization. The PMG plot to the high-Au side of the IIIAB crescent. The Ga content of PMG-am Glorieta Mountain is lower that that of the lowest IIIAB, and six PMG or anomalous PMG have Ga contents higher than those in IIIAB, the highest being in PMG-am Huckitta and Brenham. Not shown in Figure 3, the Ge-Au trends in IIIAB and PMG are similar to those for Ga; we also model these later in the paper.

The Cu plot (Fig. 3b) is interesting and somewhat surprising. There is a small, 20–30% decrease across IIIAB that overlaps the PMG with Au contents <2.1 μg/g. With two exceptions, the remaining PMG and anomalous PMG then form an upward trend that involves a Cu increase by a factor of 2, reaching 300 μg/g in Acomita and 220 μg/g in Mount Vernon. During this increase the Cu is positively correlated with Au. Elimination from the sample set all samples with low Co contents does not change the distribution; both high and low Cu values are still present. Not shown, a plot of Cu vs. Ga shows a bit of a negative trend; if, as suggested below, high Ga and Ge values reflect magmatic volatiles, the high Cu values cannot be attributed to the same process. Metallic Cu has been observed in some chondrites (Rubin, 1994) and some IAB irons (El Goresy, 1965); we suspect that some excess Cu can be attributed to a tendency to select samples containing metallic Cu.

The As-Au diagram (Fig. 3c) is remarkably linear, with most PMG clustered around the upper extreme of IIIAB. The two most deviant high points are samples with high kamacite/taenite ratios: the PMG-am is Krasnojarsk, and the PMG to its lower left at 2.6 μg/g Au is Imilac, paired with an Iimaes sample that lies along the main trend.

There is some experimental scatter on the Sb-Au diagram (Fig. 3d) but the IIIAB trend is clear; Sb values increase by a factor of ≈6 from around 25 ng/g to ≈ 150 ng/g (only anomalous Tieraco Creek reaches 180 ng/g). With the exception of a moderate value (110 ng/g) in South Bend, the PMG data form a field just beyond the high-Au extreme of IIIAB.

4.3. Compositional Classification of Main Group Pallasites

4.3.1. Normal members of the main group

Twenty (Ilimaes with Imilac) members of our set of pallasites form relatively loose "main-group" compositional clusters on Figures 2 and 3. Scott (1977a) and Davis (1977) restricted the Ir contents of normal PMG to <0.22 μg/g. If one examines the PMG cluster on the Ir-Au plot (Fig. 2d), one notes that there

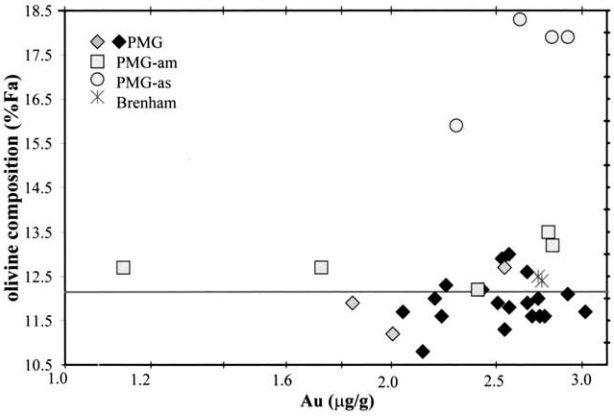

Fig. 4. Olivine fayalite contents (mainly from Buseck and Goldstein, 1969) are plotted against metal Au contents for PMG. A broad hiatus separates Argonia (13.5 mol% Fa) from four PMG having high olivine Fa (15.9–18.3 mol%) that, on this basis, are designated anomalous-silicate members of the main group (PMG-as). A line drawn at –12.15 reveals that the ten anomalous PMG all have higher Fa contents than this limit.

is a minor hiatus between a heavily populated set shown with dark diamonds (Ir <0.32 μg/g) and the outer three PMG at higher Ir contents (0.7<Ir<2.1 μg/g) shown with light diamonds. The "normal" cluster extends down to 0.017 μg/g Ir.

We list ten anomalous members of PMG; all have O-isotopic compositions similar to those in normal PMG. Four of these are defined as anomalous based on their high olivine fayalite contents. Six others (including Brenham) have metal that is anomalous in various ways described below.

4.3.2. PMG with anomalous metal compositions

We designate six PMG as PMG-am where the am stands for anomalous metal. Five are represented by gray squares in the figures, Brenham with a six-armed cross. The most extreme of these is Pavlodar, the PMG with the lowest Au content at 1.1 μg/g; the next nearest PMG is Huckitta at 1.7 μg/g. Pavlodar plots well above the IIIAB trend on the Ga-Au, Ir-Au and Pt-Au diagrams and far below the IIIAB trend on the Co-Au diagram. Davis (1977) inferred that Ir contents are similar in kamacite and taenite, thus it seems unlikely these deviations from IIIAB are mainly attributable to variations in the kamacite/taenite ratio.

Another easily locatable PMG-am is Omolon at 2.4 μg/g Au. It plots above the other PMG on Co-Au, As-Au and Sb-Au and below on Ni-Au, Cu-Au and W-Au diagrams. All of these differences are consistent with an unrepresentatively high kamacite/taenite ratio in our Omolon samples.

Krasnojarsk is the PMG with the highest contents of Co, As and Sb, and the lowest contents of Ni and Cu. The two samples had high k/t ratios, especially the first. These suggest k/t distribution ratios >1 for the former and <1 for the latter. However, our Co test, described above implies k/t <1 for Sb and indicates no trend for Cu, which Davis (1977) indicated to have a k/t >1.

PMG-am Argonia has the highest Ir content in a PMG; surprising and confusingly, the Au content (2.8 μg/g) is much

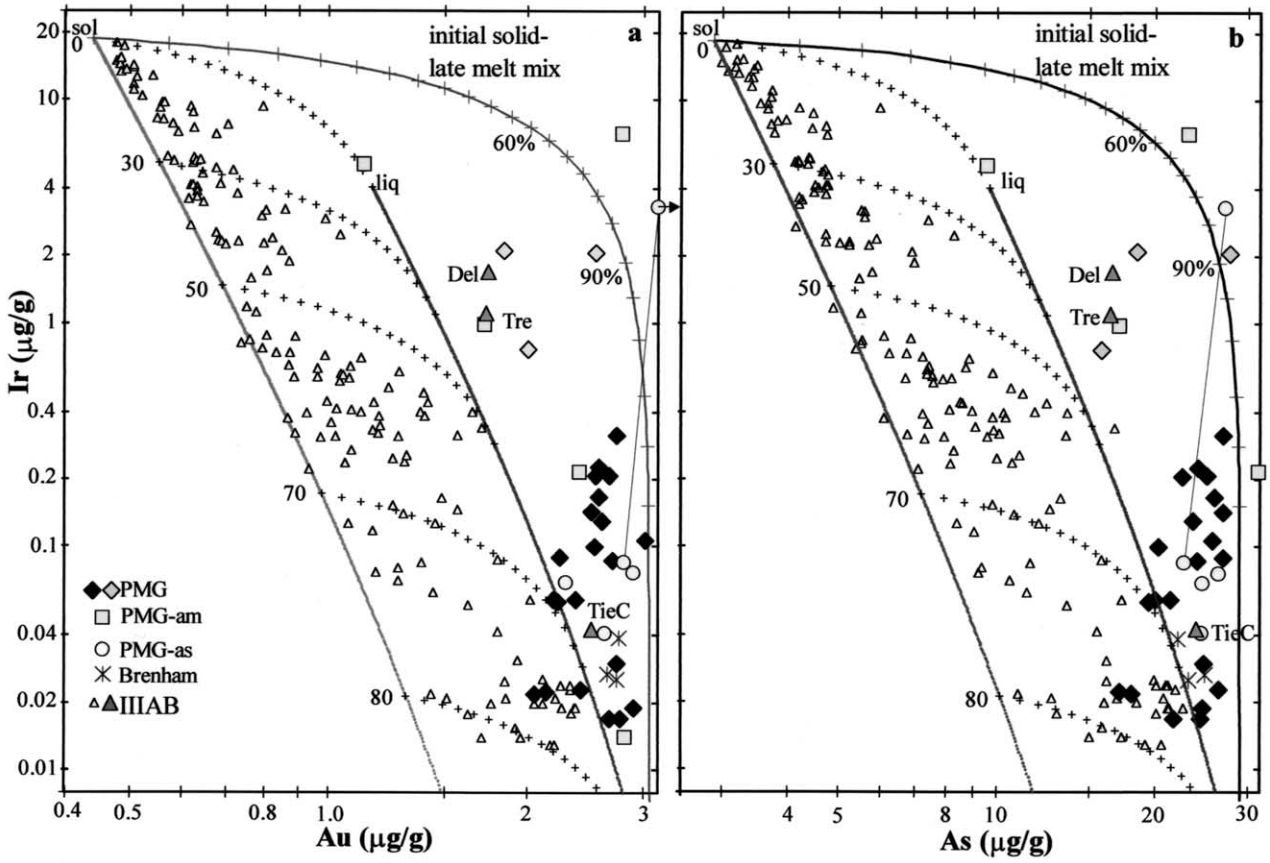

Fig. 5. Data for IIIAB and PMG are plotted together with computed IIIAB liquid and solid evolutionary tracks for (a) Ir vs. Au and (b) Ir vs. As; as discussed by Wasson (1999a), most IIIAB irons can be interpreted as mixtures of equilibrium metal and trapped melt. Such mixes are shown for 0, 30, 50, 70, and 80% crystallization; marks along the curve show 5% intervals in the mix. Scott (1977c) suggested that PMG metal could be interpreted as mixes of a late IIIAB melt and early-crystallized solids; the dark curve on the right shows a possible end member case in which the liquid evolved after 80% crystallization is mixed with initial solids. For the range 0–90% melt the marks show 5% differences in this mix; intervals are more closely spaced at higher melt fractions. With a few marginal exceptions the PMG fall to the left of this mixing curve.

higher than in other high-Ir pallasites. In other respects Argonia is a normal PMG.

The fourth PMG-am is Glorieta Mountain at 2.8 μg/g Au. The Ga and Ge contents of Glorieta are appreciably lower than those of any other PMG. The interesting thing about these new results is that Glorieta is found to plot along an extrapolation of IIIAB trends on all element-Au diagrams. In terms of the mixing model presented below, its composition is close to that expected in the evolved IIIAB melt end member. Its Ir content (0.014 μg/g), while the lowest in our PMG set, is slightly higher than our calculated liquid tracks on Figures 5a,b, suggesting minor contamination by metal having a high Ir content.

Brenham and Huckitta are exceptional chiefly in terms of their very high Ge and Ga contents; Huckitta also has elevated Pt, W and Ir; it plots very close to the IIIAB-an iron Treysa on Ir-Au and Ir-As diagrams (Fig. 5). This raises the interesting possibility that if IIIAB irons and PMG are not from the same parent bodies, Treysa and its close relative Delegate might be metal from the PMG asteroid.

4.3.3. PMG with anomalous silicate composition compositions

Four PMG are designated PMG-as because their olivine fayalite contents are much higher than those in the remaining PMG. On Figure 4 we show the fayalite content in olivine plotted against log Au. There is a hiatus in Fa between values of 13.2 and 13.5 mol% in Glorieta Mountain and Argonia, respectively, and Rawlinna, at Fa = 15.9 mol%. It is because of this large hiatus that we designated Rawlinna, Springwater, Phillips County and Zaisho as PMG-as, and show them with separate symbols (lightly shaded circles) on the diagrams.

Because of its exceptionally high troilite content, the most interesting PMG-as is Phillips County. According to Scott (1977b) the FeS/Fe ratio in this object is very high, a mol ratio of 5–10, near that present in a eutectic mixture of these phases. Unfortunately the meteorite is rather weathered. We analyzed two metal-rich samples of Phillips County and obtained very different compositions. In one of these the Au content was 4.0 μg/g (plotted with an attached arrow at 3.2 μg/g on our

compositional diagrams to increase the horizontal spread of other data points). The other sample contained 2.8 μg/g Au. The high Au sample also had higher Ir and Ni and lower Co than the low-Au sample. The two analyses are connected by lines on our diagrams. We reexamined the samples with low-power microscopy on the chance that one was contaminated, perhaps by a chip from another meteorite, but could find no evidence of such problems. We note that it is difficult to contaminate Au at such high levels in any way other than by chips of metal. The best interpretation seems to be large point-to-point variations in the metal, possibly also effects reflecting the presence of minor (including electrochemical weathering) phases in our samples; the high-Au sample had a very high Cr (i.e., chromite) content. Most of the Phillips County data plot within the PMG field but Ni is high in both samples and Ir and W are high in the high Au, high Cr sample. Some portion of the variation seems attributable to a low kamacite/taenite ratio in the sample having high Ir and Au and low Co.

Rawlinna (Fa 15.9 mol%, 2.3 μg/g Au) has the lowest Fa among the PMG-as and the highest Ni content (Fig. 2a) among our entire PMG set; its Co and Cu contents are also high. In contrast, its contents of other elements fall in the PMG cluster at the high-Au end of IIIAB.

The metal of Springwater (Fa 17.9 mol%, Au = 2.9 μg/g) is remarkably normal. Compared to the PMG cluster Co, Ni and W are slightly high, Ga and Cu are low but within the normal IIIAB range. Platinum is at the lower end of the PMG cluster.

The highest PMG Fa value is 18.3 mol% in Zaisho, whose metal contains 2.6 μg/g Au. Buseck and Clark (1984) noted that Zaisho silicates are unusual in several respects; these include phosphoran olivine and small amounts of low-Ca pyroxene in the form of symplectic intergrowths with olivine. Buseck (1977) had reported phosphoran olivine in Brahin, Rawlinna and Springwater; the latter two, like Zaisho, have high Fa. Because the high Fa implies Fe oxidation, we expected Ni and Co to be high; in fact Ni is normal though Co is slightly high. The Cu content of Zaisho metal is near the upper end of the PMG-as cluster.

4.4. Metal in the Eagle Station Pallasites

As already noted, the Eagle Station (PES) pallasites are readily resolved from the main-group pallasites (PMG) on the basis of the O-isotope compositions of their olivine. Although the chief compositional distinctions of PES metal relative to PMG metal are those mentioned above (high Ge/Ga, high Ni, high Ir), PES also have lower Au, and higher Co, Re, Pt, and Cu than PMG. Scott (1977a) reported a Co content for Cold Bay of 5.4 mg/g (contrasting with 8 mg/g in the other PES) but noted that the low Co probably reflected loss of kamacite through weathering. As discussed in the experimental section, our Cold Bay Co value (8.8 mg/g; Table 2) and other siderophile data have been corrected for loss of kamacite. This corrected Cold Bay value is similar to that in Eagle Station (8.5 mg/g) value; although our correction contributes to the total error, the final uncertainty is probably no larger than $\pm$ 0.5 mg/g.

Our compositions for Cold Bay and Eagle Station show not only that these are very closely related, they also suggest an igneous relationship between them. Relative to Eagle Station, Cold Bay has higher Ni, As and Au and lower Ir suggesting that it formed from a more evolved magma. The data of Davis (1977) for Itzawisis, the third member of the PES, are consistent with it being the least evolved (Ir-rich, Au-poor) member of the set. However, with only three detailed analyses, this igneous interpretation remains tentative.

5. MODELING THE FORMATION OF PMG METAL

In this section we adopt as a working scenario that solid mantle olivine was mixed with a highly evolved IIIAB-like liquid. This allows us to test the model proposed by Scott (1977c) to account for the loci of most PMG on an Ir-Ni diagram. The temperature of this metallic melt was probably $\sim$1600 K, $\sim$400 K less than the solidus temperature of PMG olivine having Fa = 11 mol%, thus this interpretation implies the mixing of a mobile low-viscosity metallic melt with (or injection into) crystalline olivine.

5.1. Initial S Content of the PMG Magma

As noted in the previous section, the S content of metallic magmas exercises a strong influence on distribution coefficients. In contrast to siderophiles, however, S contents of the parental magmas cannot be determined by laboratory studies of iron meteorites. Because S is incompatible with Fe-Ni metal (the solid/liquid partition ratio for S is very low, probably $<$0.02) most troilite in iron meteorites represents parental trapped liquid.

Pallasites are mixtures of cm-scale olivine and metal; $\sim$2/3 of their volume fractions are olivine, the remainder metal. In some areas all large olivine grains seem to be in contact, and in such environments it is unlikely that an FeS-rich liquid could have experienced fractional crystallization on a scale larger than the size of the interstices between grains; convection on a large scale was impossible, and diffusional transport was too slow. There is, in fact, evidence for a rapid increase in viscosity; in some areas the olivine grains appear to be suspended, i.e., not touching other olivine grains.

Modal troilite contents in PMG were measured by Buseck (1977), but most of the integrated areas were small. We used his data only for the 9 samples (including two pallasites from the Imilac shower) with areas $>$70 cm^2 and calculated the S contents in metallic (Fe-Ni and FeS) parts of the pallasites; these range from 2.3 to 41 mg/g. The highest S contents were Albin, 41 mg/g, Brenham, 30 mg/g, Springwater, 37 mg/g and Newport, 17 mg/g. These S contents are much lower than expected in a highly evolved IIIAB melt. If we use the IIIAB S content of 24 mg/g suggested by Wasson and Richardson (2001), then crystallization of 2/3 of that melt would increase the S content to $\approx$70 mg/g, and 80% crystallization to 120 mg/g. Most other modelists (e.g., Haack and Scott, 1993) have inferred much higher initial S contents for IIIAB.

Ulff-Møller et al. (1998) carried out a detailed modal analysis of a large (3000 cm^2) section of the Esquel PMG and found that it contained only 0.46 vol% troilite together with 66% vol% olivine and 32 vol% metal. If the troilite and metal abundances are representative of the metallic melt, the S content of that melt was only 3.1 mg/g. Ulff-Møller et al. (1998) suggest that a late melt was lost. They suggest that the Esquel observations imply that, after intrusion of the metallic magma

Table 3. Empirical dependence of D_X on nonmetal contents of metallic magmas.

Element	ln D (S,P = 0)	S slope	P slope
Au	−0.995	−0.129	−0.218
As	−1.238	−0.167	−0.292
Ir	1.430	−0.84	−0.19
Ga	−0.198	−1.3	−0.8
Ge	−0.286	−1.86	−0.7

into the olivine, an FeS-rich liquid either escaped (returned to the core) or formed FeS-rich pallasitic rocks that are underrepresented in the meteorite inventory.

5.2. Mixing of an Early Solid and a Late Melt

In Figure 5 we show Ir-Au and Ir-As diagrams; on each of these most of the main-group pallasites plot to the right side of the IIIAB trend. Also shown on these diagrams are possible solid and liquid trajectories for IIIAB. These were calculated by procedures similar to those used by Wasson (1999a); the chief difference is that we use the revised IIIAB initial S content of 24 mg/g proposed by Wasson and Richardson (2001). Solid/liquid distribution ratios (D values) depend on the composition of the metallic magma, with nonmetal contents playing a key role.

We used the compositional parameterization of D values of Jones and Malvin (1990):

$$\ln (D_x) = \beta \cdot \ln(1 - 2 \cdot \alpha_s \cdot X_s - 4 \cdot \alpha_p \cdot X_p) + C$$

where X_S and X_P are the mole fractions of S and P in the melt and D_X is the solid/liquid concentration ratio of element X. We followed Jones and Malvin (1990) and used 1.09 for α_s and 1.36 for α_p. Jones and Malvin (1990) recommend that β values be obtained by fitting a straight line through a plot of ln D vs. ln $(1 - 2 \cdot \alpha_s \cdot X_s)$ and β_P from a plot of ln D vs. $\ln(1 - 4 \cdot \alpha_p \cdot X_P)$. The combined slope for a melt containing appreciable amounts of S and P is assumed to be a weighted average of these (see, e.g., summary in Wasson, 1999a).

Our approach was to use the Jones-Malvin method to make preliminary estimates of D_X, then to use a trial-and-error approach to obtain modified D_X relationships that provided plausible solid and liquid tracks that could account for iron-meteorite fractionation trends (Wasson, 1999a). Because of the interlocking nature of these sets of D_X relationships we argue that our values (e.g., those summarized in Table 3) are moderately well constrained. These fits were chosen for the S and P contents we inferred to be present in group IIIAB based on other evidence.

Wasson (1999a) noted that there is considerable scatter in the laboratory D_X data, particularly if data sets from more than one research group are used. He also stated that the available data were mainly carried out at S contents that appear to be too high to be consistent with the relatively low degree of change of D_X values during the fractional crystallization of the iron-meteorite magmas.

Scott (1977c) observed that the PMG that plot to the right of the IIIAB liquid trend on an Ir-Ni diagram can be roughly modeled as mixtures of evolved PMG melt and early crystallized IIIAB metal. The same generalization applies to the PMG fields on our Ir-Au and Ir-As diagrams (Fig. 5). Although crystallization from the inside out is necessary to produce fractional crystallization, minor crystallization at the core–mantle interface would also have occurred. We would augment the Scott model by noting that the metal trapped in the olivine-rich mantle of the PMG asteroid was a residue resulting from removal of a low-melting fraction. It would therefore be expected to have an Ir-rich composition similar to that of an early solid from a metallic magma from that body, and thus produce similar trends when mixed with evolved melt.

Plotted as solid curves on the right side of the Figure 5 diagrams are the loci of mixtures of the earliest crystallized IIIAB solids and the melt resulting from 80% fractional crystallization of the magma. With the exception of the Krasnojarsk and Finmarken points on the Ir-As diagram and Argonia and Phillips County on both diagrams all PMG data plot to the left of this mixing curve. Given the large sampling errors encountered among the PMG, even the listed exceptions are marginally consistent with this simple mixing model.

Although not shown, the same mixing model can adequately account for the PMG data on plots of the refractory elements W and Pt (Figs. 2d,e) as well. Element-Au diagrams for elements such as Ni, Co, As and Sb that show strong positive correlations with Au do not provide good tests of the mixing model.

Two volatile elements, Ga and Ge, cannot be explained by this simple mixing model. As can be seen in Figure 6, mixing an evolved melt (after 80% crystallization) with initial solid yields curves that pass below the IIIAB crescents whereas, with a few exceptions that plot within the IIIAB trend, the PMG Ga-Au and Ge-Au clusters plot to the upper right of the IIIAB crescents. In constructing this diagram we used D_{Ga} and D_{Ge} relationships (Table 3) similar to those of Wasson (1999b).

It is not possible to solve these problems on Ga-Au and Ge-Au diagrams by mixing an evolved melt with an intermediate or relatively late solid. To avoid clutter we do not show this with mixing curves, but these are easily described. On both diagrams a mixture of the 80%-crystallization liquid with a solid formed after 70% crystallization would be near but slightly below the plotted equilibrium IIIAB mixing curve at 70% crystallization, and thus far to the left of most PMG points on Figures 6a,b. But, if one returns to Figure 5, one sees that the Ir contents of many PMG can only be modeled by mixing evolved melt with solids formed at less than 30% crystallization. Thus IIIAB mixing models need to explain the Ir-Au PMG loci cannot explain the Ga-Au and Ge-Au distributions.

One possible interpretation of this conundrum is that the IIIAB irons and the PMG formed in different parent bodies, with the PMG parental magma having Ga and Ge (and possibly Cu) contents 1.2–1.6× higher than those in the IIIAB magma but with other elemental concentrations essentially the same in the two magmas. Because the other links (including O-isotopes) are so strong between PMG and IIIAB we have examined other mechanisms to explain the PMG fields on Ga-Au and Ge-Au diagrams by processes occurring in the same asteroid. Because there is some possibility that Cu reflects sampling errors, we will not discuss it further.

We suggest two chemical features that could have resulted in most PMG having higher Ga and Ge contents than would be consistent with our basic picture of olivine-metal mixing oc-

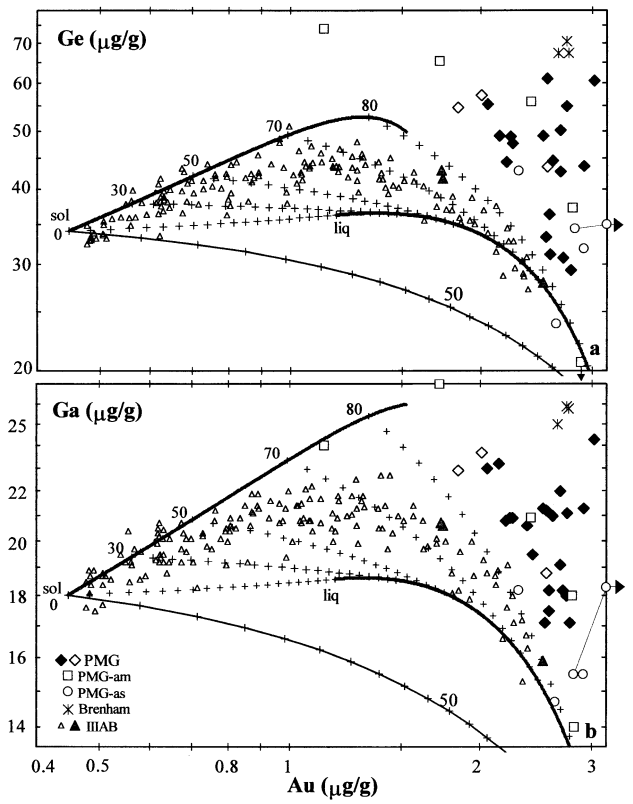

Fig. 6. Data for IIIAB and PMG are plotted together with IIIAB liquid and solid evolutionary tracks for (a) Ga vs. Au and (b) Ge vs. Au; as discussed in the Figure 5 caption, mixes are shown for 0, 30, 50, 70, and 80% crystallization, with marks along the curve showing 5% intervals in the mix. With the exception of Glorieta Mountain, which has very low Ga and Ge contents that plot near an extrapolation of the IIIAB trend, the PMG plot above and/or to the right of the IIIAB trend. The dark curve at the bottom of each diagram shows the distribution obtained by mixing 80% liquid with initial solid; in contrast to the Ir-Au and Ir-As distributions shown in Figure 5, the PMG Ga-Au and Ge-Au data cannot be explained by mixing an evolved IIIAB liquid with an early solid.

curring in a dynamic tectonic process that crushed solid mantle olivine and mixed it with an evolved IIIAB-like magma: (1) their high volatility, the highest in our set of elements; and (2) their partially lithophile nature combined with their compatibility (Ge with olivine, Ga with plagioclase).

The second possibility, that the excess Ga and Ge originated in mantle silicates, might be plausible if the PMG metal were more reducing than the mantle; both Ga and Ge are partitioned between silicates and metal and the greater the degree of oxidation, the larger the fraction in the silicates. However, the opposite situation seems to have prevailed in the PMG formation region based on the fact that the fraction of the P that is oxidized is much larger in PMG and evolved IIIAB metal compared to early crystallized IIIAB that probably preserved the original oxygen fugacity at the time of separation of the core metal from the mantle. We therefore reject this hypothesis.

In contrast, the first hypothesis, condensation of Ga and Ge from a cooling magmatic gas, is favored by the increased degree of oxidation of the PMG metal compared to early metal and the mantle. We picture the model to involve turbulent outgassing from a volume of melt many times larger than that the volume that engulfed olivine to form PMG. We suggest that the void space could have been two orders of magnitude larger than the volume of the PMG layer, which may have only been a few m thick, and that, following condensation of the gas, autooxidation/reduction produced Ge that diffused back into the metal. The formation and survival of voids is discussed below in sections 6.6 and 6.7.

As discussed by Wai and Wasson (1977) for solar nebular conditions, the volatility of Ge is increased under oxidizing conditions. Under high-temperature reducing conditions Ge is the main gaseous phase, but increases in the oxygen and sulfur fugacity can produce partial pressures of GeO and GeS that are orders of magnitude larger than that of Ge, the factor increasing with decreasing temperature and increasing O and S fugacity. In a nebula of solar composition Wai and Wasson (1977) noted that the pGeO is $10^6\times$ greater than pGe. This factor falls to 240 at 1600 K at a nebular pH_2/pH_2O ratio of 1500, but it seems probable that, in an evolved IIIAB melt, the pH_2/pH_2O ratio is several orders of magnitude lower and the pGeO/pGe ratio accordingly higher.

Wai and Wasson (1977) estimated a Ga activity coefficient of 0.1 in solid Fe-Ni metal at ca. 1000 K, and it seems likely that that for Ge is similar. However, in a highly evolved IIIAB melt the high S concentrations would probably cause the activity coefficients to be appreciably larger than unity, thus enhancing the vapor pressures of Ge and Ga. We have not carried out complete calculations of Ge and Ga volatility in part because we have not yet found free energy data for GeS, GaO and GaS, in part because detailed calculations are beyond the scope of this paper. We did a primitive calculation for an evolved IIIAB melt in which we assume a high Ge activity coefficient of 10 and a pH_2/pH_2O ratio of 1, 1500 times lower than in the nebula, and found that the Ge content of the gas at 1600 K was $\approx 10^5\times$ smaller than that of the same volume of melt. We suggest that this ratio needs to be 100 or less if the model is to work. It seems possible that we may later learn that our assumed activity coefficient was too low, our pH_2/pH_2O ratio too high or that the pGeS is as high or higher than pGeO, and that the volatility model is plausible.

Other siderophiles are much less volatile than Ge and Ge with the possible exception of Sb. A small enhancement in Sb would, however, not be easily resolved because the observed high PMG values are those expected from extrapolation of IIIAB trends.

6. FORMATION OF MAIN-GROUP PALLASITES

Because meteorites called pallasites originated on at least three parent bodies, there is no requirement that all formed by the same set of processes. If past authors did not specify otherwise, we infer that their models were meant to explain the common PMG pallasites. A variety of models have been proposed; several are summarized in Table 4. The chief features that require explanation are (1) mixtures of refractory, low-FeO olivine and metal having a much lower liquidus temperature; (2) olivine that is essentially monomineralic (i.e., why are contents of other silicates or other mesostasis phases so low); (3) the shape of the olivine: angular in 80% of the PMG, round in the remainder; (4) the unusual mix of minor minerals—

Table 4. Comparison of some models of pallasite formation, particularly the mechanisms for producing and preserving coexisting metal and olivine.

Reference	Olivine-metal mixing scenario	Notes
Rayleigh (1942)	Olivine trapped under mantle roof	Angular olivine primitive
Urey (1966)	Olivine suspended in low-gravity field near center of core	
Wasson and Wetherill, 1968	Mixing results from collapse of mantle shell	Angular olivine primitive
Scott, 1977a,b,c		Angular olivine primitive
Wood, 1978a,b, 1981	Molten metal replaces molten basaltic mesostasis	Round olivine primitive
Malvin et al., 1985	Impact generation of magma, rapid cooling (model for PES only)	
Scott and Taylor, 1990	Impact mixing for PMG with angular olivine, wood model for round olivine	
Ulff-Møller et al., 1998	Collapse of mantle or impacts, rapid increase in viscosity on cooling	

troilite, schreibersite, chromite, phosphates, low-Ca pyroxene and phosphoran olivine; (5) the anomalous high Ga and Ge contents of the metal and the high fayalite contents of the olivine in PMG having the same O-isotope composition as normal PMG.

6.1. PMG Olivine as a Mantle Cumulus

There were early suggestions that pallasites formed at the center of a core (Rayleigh, 1942; Urey, 1966), but the arguments against such an origin are very strong (Wasson and Wetherill, 1968; Scott, 1977a) and there is no longer serious discussion of formation at locations other than the core–mantle interface between a crystallizing metallic magma and the surrounding solid mantle. In the following discussion we will describe the magma body as a central core, but we recognize that magmas may have formed at locations other than the center of parent bodies, particularly if impact heating was involved. Such an impact-generated magma was suggested by Malvin et al. (1985) for the Bocaiuva iron and its pallasitic relatives, the PES.

Many lines of evidence indicate that the PMG formed at a core–mantle interface. The olivine is very coarse; according to Scott (1977b) the largest olivine grains (in Mount Vernon) reached sizes ≥30 cm; Ulff-Møller et al. (1998) describe fractured olivines in Esquel that were originally single crystals ≥20 cm in length.

The very low abundance in PMG silicates of incompatible-lithophile tracers of trapped silicate liquid (Masuda, 1968) implies formation as a cumulate at the bottom of a slowly cooling silicate magma chamber. Buoyant separation is enhanced by stronger gravitational fields, thus this implies formation at moderate distances from the center of the body (we suggest >5 km). The chondrite normalized rare-earth element (REE) abundances in pallasitic olivine show an olivine pattern with a chondrite-normalized ratio of $2 \cdot 10^{-2}$ near Dy-Ho (Masuda, 1968), and expected for a nearly pure cumulus with minimal trapped mesostasis precipitated from a magma having a roughly chondritic REE pattern. However, PMG silicates studied by Schmitt et al. (1964) show higher REE abundances and no pronounced olivine pattern. Because phosphates are common in PMG and the REE tend to concentrate in these when they are present (Davis and Olsen, 1991, 1996), it is difficult to obtain meaningful whole-rock REE concentrations from small pallasite samples.

6.2. Primacy of Angular Olivine: Evidence for Olivine Crushing during Melt Intrusion

As discussed by Scott (1977b), the olivine of most pallasites is angular and there is little doubt that the common, small, angular olivine was formed by fragmentation of larger masses. In most pallasites the smallest olivines are round. With rare exceptions, the size distribution appears to be truncated at a size of ~20 μm, implying that smaller sizes were unstable during metamorphism; their constituents diffused to and were deposited on the surfaces of larger crystals to minimize surface energies. The largest (20–30 cm) olivine masses are often criss-crossed by metal-filled cracks (Davis, 1977; Ulff-Møller et al., 1998). A minor fraction of the pallasites contain rounded olivine. Some large olivine masses show 120° junctions between olivine grains 1–2 cm across, implying that this is the original grain size. In our opinion, there is no doubt that the angular olivine is the original form.

6.3. Generation of the Large Range in FeO/(FeO + MgO) Ratios in the Olivine of PMG and PMG-as

The fayalite contents of PMG olivine are plotted against Au in Figure 4. Most fall in the range 11.2 to 13.5 mol%, but four have compositions in the range Fa16–18 (Buseck and Goldstein, 1969; Buseck and Clark, 1984). These PMG-as differ from normal PMG mainly in terms of their high Fa contents in olivine; at least three of them contain phosphoran olivine (Buseck 1977; Buseck and Clark, 1984). In addition, as shown in Figure 4, all five PMG-am have Fa >12.15%.

As discussed above, oxygen isotope compositions of PMG-as fall in the normal PMG range. All our PMG-as have Ir concentrations in the normal range. Most other siderophile compositions also fall in the PMG range; the exceptions are Co and Ni, which are marginally higher than in normal PMG. Because variations in the kamacite/taenite ratio cause concentrations of these elements to vary inversely, the fact that both are high suggests that Fe was removed from the metal as a result of oxidation.

These similarities between high-Fa and normal PMG suggest that they formed in same parent body, despite their difference in Fa contents. We considered two possible formation scenarios, (1) olivine in the high-Fa pallasites is a later-crystallized solid from the magma that produced the olivine in normal PMG

pallasites; or (2) oxidation of Fe to FeO occurred in connection with the intrusion of the metallic liquid in this region.

We doubt that it is possible to create a plausible evolutionary sequence that would yield the first scenario. If the change from Fa11 to Fa18 was the result of igneous fractionation of the mantle melt, this would have required that the Fa18 olivine formed after ~30% of the silicate magma had crystallized. However, after this amount of crystallization it is probable that pyroxene (which is a negligible component of PMG-as) would have been a liquidus phase. And, if the magmatic layer was originally >10 km thick, this Fa18 olivine would have formed >3 km above the core–mantle interface. If the olivine is mainly a residue from incomplete melting of the precursor (probably chondritic) materials, the distance required to reach such evolved olivine would be still larger. It seems improbable that such distant mantle materials would have been mixed with the core melt. In contrast, the elevated Co and Ni contents of the metal of several PMG-as imply that Fe was removed by oxidation. We thus find the second model plausible and substantially more probable than the first.

There appears to be a tendency for contents of phosphoran olivine to be higher in PMG-as than in other PMG (the exception is Brahin, here called a normal PMG, but very rich in Ga and Ge). This is more easily explained with the second scenario, since the introduction of PO_4^{-3} into the olivine compensates for the additional amount of +2 cations associated with oxidizing Fe to Fe^{+2} in these essentially pyroxene-free meteorites. This suggests a scenario in which the extra oxidizing capacity is carried by a magmatic gas phase. If we are correct that the enhanced Ga and Ge in PMG reflects condensation from such a phase, then one might expect higher Ga and Ge in the PMG-as compared to normal PMG, but no correlated enhancement is observed. This may mean that the gas-source model is incorrect, but we suggest the following alternative. Because the Ga and Ge enhancement is observed in metal and the Fa effect in silicates, it is possible that the latter effect is more noticeable in regions having high metal/silicate ratios, the Ga and Ge enhancements are greater in regions having low metal/silicate ratios, thus accounting for the lack of a strong correlation.

6.4. Evolution of IIIAB-like Cores: Formation of High-Ir PMG

As discussed in section 5, our metal data (Figs. 2, 3) show that PMG have compositions differing from the main IIIAB trend chiefly in ways consistent with higher mean degrees of crystallization, higher mean contents of trapped melt, and contamination by refractory-rich solids (early metal crystallites (Scott, 1977c) or mantle residues). Our working assumption is that PMG refractory siderophile trends are best explained in terms of such a model.

The high efficiency of the IIIAB fractional-crystallization process (Ir concentrations decline across the group by a factor of 2000) implies that the residual melt remained thoroughly mixed throughout the crystallization process. As emphasized by Wasson (1972, 1985), this mixing of the core is most efficiently achieved by crystallization from the center outwards, convection being aided by liberation of latent heat and light elements (such as S) at the point of crystallization. The generally low Ir contents of metal in normal PMG implies that the evolved IIIAB-like parental melt was largely located near the core–mantle interface, consistent with crystallization of the core from the center outwards.

Although Haack and Scott (1992, 1993) interpreted the structure of the Agpalilik specimen of Cape York and the Savik-Agpalilik chemical trends to imply the formation of dendrites growing downward from the core mantle interface, Esbensen et al. (1982) and Wasson (1999a) explained the Cape York structural and chemical trends by a tectonic mixing process and variations in the fraction of trapped melt. Even though we think it likely that the core crystallized from inside to out, it seems clear that some minor fraction of the initial, Ir-rich solids would have nucleated at the core–mantle boundary. The earliest crystallized members of group IIIAB are Rateldraai (19 μg/g Ir) and Picacho (20 μg/g Ir).

Olivine, the major silicate mineral of pallasites, is the main mineral phase expected in the mantle of an asteroid. Therefore the common PMG model involves the mixing of solid olivine mantle and residual metallic liquid after most of the core had crystallized to form IIIAB-like irons. Because, after mixing, pallasitic olivine did not separate from the metallic liquid, the melt could not subsequently have undergone large scale convection-driven fractionation. Although minor gradients would have formed as each small melt pocket crystallized (and, as discussed by Ulff-Møller et al. (1998), frequently lost the last FeS-rich melt), these would have been flattened by diffusion in the slowly cooling ($\approx$50 K Ma^{-1}) planet.

Concentrations of Ir show a wide range within the PMG. The two with the highest Ir contents are PMG-am Argonia (6.5 μg/g Ir) and Pavlodar (5.2 μg/g Ir); their Ir contents can be explained by mixing 30% metal with a composition like IIIAB Rateldraai (19 μg/g Ir) with 70% of the evolved melt. The next highest values are in the range from 2.1 to 0.8 μg/g Ir; these plot close to the anomalous IIIAB irons Treysa and Delegate. There is a sizable gap (from 0.32 to 0.76 μg/g) between these and normal PMG. Other elements show minor or negligible differences between high-Ir and normal PMG (Pavlodar, with low contents of Au, etc., is the exception).

Scott and Taylor (1990) suggested that high-Ir PMG-am (and Pavlodar in particular) might be derived from a separate asteroid from PMG, but give no basis for this suggestion other than the Ir content. Because Pavlodar is so different in composition from the other PMG, we agree that it probably formed in a somewhat different environment. However, because it plots close to the IIIAB trend on all diagrams, our preferred hypothesis is that it is from the same parent body. We nonetheless plan to determine its O-isotopic composition.

As noted above, the core–mantle boundary is expected to be one site for initial metal crystallization, i.e., some refractory metal must have nucleated on the olivine-mantle roof. This suggests one mechanism to account for the high-Ir PMG-am. When mechanical mixing between olivine and residual metallic liquid occurred to form normal PMG, some samples could have been "contaminated" by early-solidified metal (either because it was already in contact with the olivine or was eroded and entrained during the flow of magma through cracks in their shell of "wall-rock" metal). Alternatively, the high-Ir metal could be a minor refractory residue that had remained in the mantle after most metal had drained out of the mantle to form the core.

6.5. Formation Temperatures of Pallasites

The typical, angular olivine texture implies that olivine was solid and metal liquid when they were mixed. To estimate the temperature of the metallic melt within a narrow range we must know its composition, particularly its S content. If we use the initial IIIAB S content (24 mg/g) discussed in section 5 and assume that the core had experienced ≤80% crystallization at the time the PMG mixing event occurred, we obtain a S content of ≤120 mg/g for the PMG magma; it appears that most pallasites could be modeled with a somewhat less evolved melt, perhaps having a S content of 100 mg/g. Solidus temperatures of FeS melts containing 100 and 120 mg/g S read off Fe-S phase diagrams (e.g., Brandes and Brook, 1992) are ≈1650 and ≈1630 K, respectively. Because the presence of appreciable P and Ni will further depress the melting temperature, we suggest a probable melt temperature of 1600 K with an uncertainty of 20–30 K.

6.6. Olivine-Metal Mixing Event

In this section we discuss physical models to account for the nature of the pallasitic texture, which is a mixture of olivine and metal having large difference in densities and melting temperatures. The significance of the distribution of PMG olivine into angular or rounded shapes is also addressed. It is appropriate to briefly review past ideas about the processes that created the pallasitic mix of olivine and metal; some important papers are summarized in Table 4.

The first modern paper was that of Rayleigh (1942), who stated that angular olivine fragments were primary, and inferred that pallasites formed by buoyant solid olivine rising through molten metal until they became trapped beneath a ceiling. He proposed that round olivine formed from angular olivine by abrasion.

Wood (1978a,b, 1981) focused his attention on the fall statistics of PMG and IIIAB irons to estimate the fraction of pallasitic material in the IIIAB parent body. In his model pallasites are assumed to have resulted from the submersion of olivine crystals into a metallic magma as the result of overburden pressure. This approach is largely based on the assumption that round olivine crystals are the primary form, and that they were initially separated by an intercumulus silicate liquid, which was later replaced by the metallic melt. Wood (1981) concludes that this buoyancy model is most easily understood if the asteroid radius was around 10 km, whereas the low metallographic cooling rates imply an asteroidal radius ≥150 km. His suggests that his scenario can be made to work but that it demands special circumstances.

There are several reasons to be skeptical about Wood's model. Chief among these is the fact that most pallasites consist of fragmental olivine, implying a high-energy mixing event. It also seems highly unlikely that a basaltic intercumulus liquid could have been present in the mantle when the metal-olivine mixing event occurred. Such an intercumulus liquid is not unreasonable if the temperatures (ca. 1600 K) estimated above for the metallic liquid at the time it mixed with the silicate are taken to be maximum temperatures reached in the core and mantle. However, the parent body must have experienced much higher temperatures at the time the core formed. If we assume that the initial S content of the core was 24 mg/g (Wasson and Richardson, 2001), the inferred minimum temperature at core separation was ≈1750 K. At this temperature a chondritic (e.g., H-chondrite) precursor would have experienced >30% melting of silicates, including all the plagioclase and most or all of the pyroxene (Taylor, 1992). Such a melt should have separated upwards at the time the metal was migrating downwards. Thus Wood's suggestion that there was 30–40 vol% silicate liquid present at the time the metal mixed with the olivine is implausible. A final implausibility of Wood's model is that its illustrative cartoons seem to show that the metal in the pallasites should have the mean composition of IIIAB irons whereas the observed metal composition is close to that of a highly evolved (80%-crystallized) IIIAB magma.

Scott and Taylor (1990) accepted Wood's static model as the best explanation for PMG with round olivine but concluded that the common pallasites having angular olivine required impact mixing and rapid chilling of the metal. It is certainly true that long immersal in molten metal would yield an environment conducive to rounding but the key question is then why some PMG regions stayed hot longer than others. We see no connection between this question and Wood's suggested replacement of a basaltic intercumulus liquid with metal.

In a lengthy paper Wasson and Wetherill (1968) also concluded that angular olivine was primary. They noted that the solidification of an initially molten core would lead to a 2% volume contraction, corresponding to a 0.7% linear contraction. Although the olivine mantle and the solidified part of the core both contracted (to roughly similar degrees) during cooling, the contraction of the core resulting from its solidification would leave the mantle unsupported. For example, if the core radius were 10 km, the linear contraction due to solidification would correspond to 70 m. Although some tectonic readjustment of the mantle must have occurred throughout the core solidification, it is plausible that one of the most dramatic collapse events (perhaps triggered by an impact on the surface of the asteroid) was the one that formed the PMG.

Mantle collapse offers a simple mechanism to produce the voids hypothesized in connection with the inferred role of magmatic gas. We suggested above that "contamination" by condensates from a magmatic gas phase was responsible for the enhanced Ga and Ge contents of the PMG and also for the oxidation of Fe recorded in the PMG-as. A series of mantle collapse events probably occurred during core crystallization; these would have produced large amounts of voids. As discussed in the following section, if the asteroid was relatively small, the combination of overburden pressure and temperature would have allowed these voids to survive for an extended period. As the parent body cooled, pallasitic regions near the cavity-rich mantle would have experienced larger "contamination" effects from these magmatic condensates than would have those near cavity-poor regions. We picture that the abundance of cavities was heterogeneous on a scale of meters to tens of meters.

6.7. Fragmentation, Density and Insulation in a Rubble-Pile IIIAB-PMG Asteroid

Recent spacecraft determinations of the densities of small asteroids have yielded surprisingly low densities. 253 Mathilde

was found to have a density of only 1.3 g cm^{-3} (Veverka et al., 1999); if its void-free density is that of a typical ordinary chondrite, ~3.6 g cm^{-3}, the porosity is 64%. 433 Eros has a density of 2.67 g cm^{-3} (Veverka et al., 2000; if it is an ordinary chondrite as suggested by its spectrum and composition, its porosity is 26%. Although more studies are required, there is a developing consensus that most small asteroids have high porosities, perhaps averaging around 30–50%.

It is important to note that asteroids having high micro- and macro-porosities will also have low thermal conductivities, perhaps by as much as an order of magnitude. As a result, sizes of the IIIAB-PMG parent body inferred from cooling rates when the body cooled through the range 800–600 K may be too high.

Wasson and Kallemeyn (2002) suggested that impact heating can melt large regions within highly porous bodies. In contrast to heating by radioactive sources, this offers the possibility for having regions of melt inside asteroids which also preserve macroporosity in the same general region. Because of the high strength of rocky materials and low gravitational fields of small asteroids, the presence of a large melt body is not inconsistent with the presence of macroporosity.

For modeling purposes we need to assess the radius of the parental asteroid. Rasmussen (1989) used metallurgical data to estimate a mean cooling rate of 49 K/Ma for group IIIAB. Using an asteroid model that included a thin regolith he calculated a radius of 25 ± 7 km. We therefore suggest that the radius R of the PMG parent asteroid was relatively small, perhaps between 10 and 50 km.

To calculate the overburden pressure we used the following expression derived for bodies having uniform densities; there is only a minor difference in pressure at the core–mantle boundary compared to an exact calculation involving a high-density core surrounded by a low-density mantle:

$$P\ (atm) = 1.379 \cdot 10^{-3} \cdot \rho^2 \cdot (R^2 - r^2) \quad (1)$$

Here ρ is the density (g cm^{-3}) and r is the radial distance of the region of interest from the center of the asteroid. We considered only the case where r = R/2; this corresponds to the core occupying 12.5% of the volume and (if the core density is 7 and the mantle density is 3 g cm^{-3}) to 25% of the mass. We made two limiting calculations. To calculate a maximum pressure we set R = 50 km and ρ = 3.5 g cm^{-3}; this yields P = 24 atm (2.4 MPa). As a minimum pressure we set R = 10 km and (as a rough rubble-pile density) ρ = 2.0 g cm^{-3}; this gave a pressure of 0.4 atm (0.04 MPa).

We suggested above that gas entrapment in voids might offer an explanation of the anomalously high Ga and Ge contents in most PMG as well as high Fa contents in the olivine of PMG-as by chemical changes resulting from reactions with components of the gas phase associated with the metallic magma. A key question is then how long such macroporosity can exist before the cavities are collapsed by creep.

Fowler (1985) noted that rate of collapse of the fractional porosity f is related to the overburden pressure (p) and the viscosity (η) by the formula:

$$df/dt = -f - p/\eta \quad (2)$$

Integration of this formula shows that the fractional porosity decreases by a factor of 2 within the period 0.693 · (η/p).

The largest unknown in this equation is the viscosity of dry olivine at 1600 K, the temperature estimated in section 6.5. There is no doubt that the asteroid would be in the diffusional creep regime. We will use 10^{21} poise or (10^{20} Pa-s) calculated from eqn. 2 of Hirth and Kohlstedt (1996); the main uncertainty is the differential stress which we set equal to the overburden pressure. Incorporation of the above two limiting pressures into Eqn. 2 gives a half-lives for collapse of 0.7 Ma at 24 atm and 52 Ma at 0.4 atm.

Our calculations show that the GeO vapor pressure of decreases by a factor of ~2.5 if the temperature is reduced by 100 K, an order of magnitude if the temperature falls ~260 K. Low-temperature metallurgical cooling rates of 50 K/Ma correspond to cooling rates of ca. 100 K/Ma at 1600 K, thus the partial pressure of GeO in a void should drop by an order of magnitude in 2.6 Ma. During this period the volume reduction due to creep would be ~93% for the dense 100-km-diameter asteroid, but only <1% in the small rubble-pile asteroid. We suggest that 93% collapse poses no significant problem for our model although longer half-lives are more favorable.

7. SUMMARY AND CONCLUSIONS

Our compositional data for metal from the main-group pallasites (PMG) support earlier views that these formed at the core–mantle interface of an asteroid. Our data are generally consistent with the idea that the PMG formed in the IIIAB asteroid; most PMG have compositions close to those inferred for evolved IIIAB melt present after 75–80% crystallization of the IIIAB core. All samples were analyzed two or more times by INAA; the resulting higher precision has reduced the degree of scatter compared to previous studies of the PMG. Despite these improvements, the PMG show more scatter than present in a similar-size set of evolved IIIAB irons.

The chief problems with forming the PMG in the IIIAB asteroid are the elevated contents of refractory siderophiles (e.g., Ir) in numerous PMG and the high contents of Ga and (especially) Ge in most PMG compared to those expected in evolved IIIAB liquids. Scott (1977c) noted that the former could be explained by mixing evolved IIIAB melt with an early crystallized IIIAB solid. Our more extensive and precise data support this interpretation. We suggest the minor modification that, because mantle residual metal also had high Ir contents, it could have served as the refractory end member in this mixing model.

In our data set the mixing model can account for all but two PMG element-Au fields on element-Au diagrams. The exceptions are Ga and Ge, whose position on these diagrams are much (≈1.5× for Ga, ≈3× for Ge) higher than predicted. Because these are the only siderophile data that are inconsistent with the interpretation that PMG formed in the same asteroid as the IIIAB irons, we examined other mechanisms to account for these data within that asteroid. Our proposal is that appreciable amounts of Ga and Ge were present in the gas phase associated with the metallic melt and that, after cooling and condensation, these materials "contaminated" the PMG.

In most PMG the FeO/(FeO + MgO) mol ratio in olivine is 0.11–0.13, but four PMG-as have values in the 0.16–0.18 range. This increase is too large to explain by fractionation of the silicate magma. The degrees of fractionation (perhaps 30%)

that such a model demands are too high to be consistent with olivine formation near the bottom of the mantle, an additional problem is that pyroxene should be a liquidus phase in such an evolved magma. We therefore examined the possibility that this reflects oxidation that postdates the mixing of the olivine and metal. We suggest that the gas associated with the metallic melt had a much higher oxygen fugacity that that present at the core–mantle interface at the time of core separation (O is highly incompatible in metallic Fe), and that this gas (or its condensation products) was the oxidizing agent that resulted in some Fe being oxidized to the $+2$ state and some P being oxidized from the -3 to the $+5$ state.

We join the majority of past pallasite researchers in concluding that angular olivine is the primary form. This suggests that pallasites formed in high-energy events that crushed mantle olivine and mixed it with residual melt from a IIIAB-like core. We also agree with those who attribute this mixing to impacts, but we note that differential contraction of the molten core relative to the solid mantle could have led to structural instabilities that contributed to impact-induced collapses.

We further suggest that the collapse of the mantle may have resulted in appreciable voids, and that these would have contained a magnatic gas phase that contributed to the enhanced Ga and Ge contents of PMG metal and the high degree of oxidation of the PMG-as, which have FeO/(FeO + MgO) ratios $1.5\times$ higher than those in the "normal" PMG.

An asteroid with high micro-and macro-porosity could have had a thermal conductivity an order of magnitude lower than that of a low-porosity body. As a result, the low ($\approx$10 K Ma^{-1}) cooling rates in PMG and IIIAB irons may not be inconsistent with the formation of these in relatively small ($20 < R < 100$ km) asteroids.

Acknowledgments—The analyses reported here have been carried out by numerous members of our research group including J. Willis, D. Malvin, J. Wang, E. Jerde and K.L. Robinson. We thank W. Moore, A. Treiman, A. Brandon, and especially A. Davis for advice and constructive criticism. Technical assistance was rendered by a large set of UCLA undergraduates, including J. Hong, R. Hua, K. Jo, L. Lee, J. Tran, S.-B. Yoo and S. Zhang. This research was mainly supported by NASA grant NAG5-10421 and its predecessors and successor and by Korea Research Foundation Grant (KRF-2000-015-DS0045: Choi).

Associate editor: A. Brandon

REFERENCES

Afiattalab F. and Wasson J. T. (1980) Composition of the metal phases in ordinary chondrites: Implications regarding classification and metamorphism. *Geochim. Cosmochim. Acta* **44**, 431–446.

Boesenberg J. S., Prinz M., Weisberg M. K., Davis A. M., Clayton R. N., Mayeda T. K., and Wasson J. T. (1995) Pyroxene pallasites: A new pallasite grouplet (abstract). *Meteoritics* **30**, 488–489.

Boesenberg J. S., Davis A. M., Prinz M., Weisberg M. K., Clayton R. N., and Mayeda T. K. (2000) The pyroxene pallasites, Vermillion and Yamato 8451: Not quite a couple. *Meteor. Planet. Sci.* **35**, 757–769.

Brandes E. A. and Brook G. B. (1992) *Smithells Metal Reference Handbook.* 7th ed. Butterworth-Heinemann.

Buseck P. R. (1977) Pallasite meteorites—Mineralogy, petrology and geochemistry. *Geochim. Cosmochim. Acta* **41**, 711–740.

Buseck P. R., Moore C. B., and Goldstein J. I. (1967) Marburg—A new pallasite. *Geochim. Cosmochim. Acta* **31**, 1589–1593.

Buseck P. R. and Goldstein J. I. (1969) Olivine compositions and cooling rates of pallasitic meteorites. *Bull. Geol. Soc. Am.* **80**, 2141–2158.

Buseck P. R. and Holdsworth E. (1977) Phosphate minerals in pallasite meteorites. *Min. Mag.* **41**, 91–102.

Buseck P. R. and Clark J. (1984) Zaisho—A pallasite containing pyroxene and phosphoran olivine. *Min. Mag.* **48**, 229–235.

Clayton R. N. and Mayeda T. K. (1996) Oxygen isotope studies of achondrites. *Geochim. Cosmochim. Acta* **60**, 1999–2017.

Davis A. M. (1977) The cosmochemical history of the pallasites. Thesis. Yale University.

Davis A. M. and Olsen E. J. (1991) Phosphates in pallasite meteorites as probes of mantle processes in small planetary bodies. *Nature* **353**, 637–640.

Davis A. M. and Olsen E. J. (1996) REE patterns in pallasite phosphates—A window on mantle differentiation in parent bodies. *Meteor. Planet. Sci.* **31**, A34–A35.

El Goresy A. (1965) Mineralbestand und Strukturen der Graphit- und Sulfideinschlüsse in Eisenmeteoriten. *Geochim. Cosmochim. Acta* **29**, 1131–1151.

Esbensen K. H., Buchwald V. F., Malvin D. J., and Wasson J. T. (1982) Systematic compositional variations in the Cape York iron meteorite. *Geochim. Cosmochim. Acta* **46**, 1913–1920.

Fowler A. C. (1985) A mathematical model of magma transport in the asthenosphere. *Geophys. Astrophys. Fl. Dyn.* **33**, 63–96.

Francis C. A. and Lange D. E. (1987) A new olivine-chromite assemblage in the Brenham pallasite (abstract). *Geol. Soc. Abst. Prog.* **19**, 667.

Haack H. and Scott E. R. D. (1992) Asteroid core crystallization by inward dendritic growth. *J. Geophys. Res.* **97**, 14727–14734.

Haack H. and Scott E. R. D. (1993) Chemical fractionations in group IIIAB iron meteorites: Origin by dendritic crystallization of an asteroidal core. *Geochim. Cosmochim. Acta* **57**, 3457–3472.

Hirth G. and Kohlstedt D. (1996) Water in the oceanic upper mantle: Implications for rheology, melt extraction and the evolution of the lithosphere. *Earth Planet. Sci. Lett.* **144**, 93–108.

Jones J. H. and Malvin D. J. (1990) A nonmetal interaction model for the segregation of trace metals during solidification of Fe-Ni-S, Fe-Ni-P, and Fe-Ni-S-P alloys. *Metall. Trans.* **21b**, 697–706.

Malvin D. J., Wasson J. T., Clayton R. N., Mayeda T. K., and Curvello W. S. (1985) Bocaiuva—A silicate-inclusion bearing iron meteorites related to the Eagle station pallasites. *Meteoritics* **20**, 257–272.

Masuda A. (1968) Lanthanide concentrations in the olivine phase of the Brenham pallasite. *Earth Planet. Sci. Lett.* **5**, 59–62.

Ramdohr P. (1965) Uber Mineralbestand von Pallasiten und Mesosideriten und einige genetische Uberlegungen. *Monatsh Deutsch. Akad. Wissenschaften Berl.* **7**, 923–938.

Rasmussen K. L. (1989) Cooling rates of group IIIAB iron meteorites. *Icarus* **80**, 315–325.

Rayleigh L. (1942) The stone-iron meteorites called pallasites: A synthetic study of their structure and probable mode of formation. *Proc. R. Soc. Lond. A* **179**, 386–393.

Rubin A. E. (1994) Metallic copper in ordinary chondrites. *Meteoritics* **29**, 93–98.

Schmitt R. A., Smith R. H., and Olehy D. A. (1964) Rare-earth, yttrium and scandium abundances in meteoritic and terrestrial matter—II. *Geochim. Cosmochim. Acta* **28**, 67, 1–86.

Scott E. R. D. (1977a) Formation of olivine-metal textures in pallasite meteorites. *Geochim. Cosmochim. Acta* **41**, 693–710.

Scott E. R. D. (1977b) Geochemical relationships between some pallasites and iron meteorites. *Min. Mag.* **41**, 265–272.

Scott E. R. D. (1977c) Pallasites-metal compositions, classification, and relationship with iron meteorites. *Geochim. Cosmochim. Acta* **41**, 349–360.

Scott E. R. D. and Wasson J. T. (1976) Chemical classification of iron meteorites—VIII. Groups IC, IIE, IIIF and 97 other irons. *Geochim. Cosmochim. Acta* **40**, 103–115.

Scott E. R. D. and Taylor J. G. (1990) Origins of pallasites at the core–mantle boundaries of asteroids (abstract). *Lunar Planet. Sci.* **21**, 1119–1120.

Sears D. W. and Axon H. J. (1976) Metal of high Co content in LL chondrites. *Meteoritics* **11**, 97–100.

Smith J. V., Steele I. M., and Leitch C. A. (1983) Mineral chemistry of the shergottites, nakhlites, Chassigny, Brachina, pallasites and ureilites. *J. Geophys. Res. (Suppl.)* **88,** *14*, B229–B236.
Taylor G. J. (1992) Core formation in asteroids. *J. Geophys. Res.* **97**, 14717–14726.
Ulff-Møller F., Choi B.-G., Rubin A. E., Tran J., and Wasson J. T. (1998) Paucity of sulfide in a large slab of Esquel: New perspectives on pallasite formation. *Meteor. Planet. Sci.* **33**, 331–227.
Urey H. C. (1966) Chemical evidence relative to the origin of the solar system. *Monthly Notices R. Astron. Soc.* **131**, 199–223.
Veverka J., Thomas P., Harch A., Clark B., Bell J. F., Carcich B., and Joseph J. (1999) NEAR encounter with asteroid 253 Mathilde: Overview. *Icarus* **140**, 3–16.
Veverka J., et al. (2000) NEAR at Eros: Imaging and spectral results. *Science* **289**, 2088–2097.
Wai C. M. and Wasson J. T. (1977) Nebular condensation of moderately volatile elements and their abundances in ordinary chondrites. *Earth Planet. Sci. Lett.* **36**, 1–13.
Wasson J. T. (1972) Parent-body models for the formation of iron meteorites. *Proc. Int. Geol. Cong.* **24,** *15*, 161–168.
Wasson J. T. (1974) *Meteorites—Classification and Properties.* Springer.
Wasson J. T. (1985) *Meteorites: Their Record of Early Solar System History*. Freeman.
Wasson J. T. (1999a) Trapped melt in IIIAB irons; solid/liquid elemental partitioning during the fractionation of the IIIAB magma. *Geochim. Cosmochim. Acta* **63**, 2875–2889.
Wasson J. T. (1999b) The trapped melt model of formation for IIIAB irons: Ga-Au and Ge-Au trends (abstract). *Lunar Planet. Sci.* **30**, 1877.
Wasson J. T. and Kimberlin J. (1967) The chemical classification of iron meteorites—II. Irons and pallasites with germanium concentrations between 8 and 100 ppm. *Geochim. Cosmochim. Acta* **31**, 2065–2093.
Wasson J. T. and Wetherill G. W. (1968) *Physical and Chemical Processes Involved in the Formation of the Iron Meteorites.* Deposited 1972 as NAPS Document 01742. Available from National Auxiliary Public Service, c/o CCM Information.
Wasson J. T. and Sedwick S. P. (1969) Possible sources of meteoritic material from Hopewell Indian burial mounds. *Nature* **222**, 22–24.
Wasson J. T., Ouyang X., Wang J., and Jerde E. (1989) Chemical classification of iron meteorites: XI. Multi-element studies of 38 new irons and the high abundance of ungrouped irons from Antarctica. *Geochim. Cosmochim. Acta* **53**, 735–744.
Wasson J. T. and Ouyang X. (1990) Compositional range in the Canyon Diablo meteoroid. *Geochim. Cosmochim. Acta* **54**, 3175–3183.
Wasson J. T., Lange D. E., Francis C. A., and Ulff-Møller F. (1999) Massive chromite in the Brenham pallasite and the fractionation of Cr during the crystallization of asteroidal cores. *Geochim. Cosmochim. Acta* **63**, 1219–1232.
Wasson J. T. and Richardson J. W. (2001) Fractionation trends among IVA iron meteorites: Contrasts with IIIAB trends. *Geochim. Cosmochim. Acta* **65**, 951–970.
Wasson J. T. and Kallemeyn, G. W. (2002)The IAB iron-meteorite complex: A group, five subgroups, numerous grouplets, closely related, mainly formed by crystal segregation in rapidly cooling melts. *Geochim. Cosmochim. Acta* **66,** 2445–2473.
Willis J. (1980) The bulk composition of iron meteorite parent bodies. Ph.D. Thesis. University of California, Los Angeles.
Wood J. A. (1978a) Nature and evolution of the meteorite parent bodies: Evidence from petrology and metallurgy. In *Asteroids: An Exploration Assessment* (eds. D. Morrison and W. C. Wells), pp. 45–55. NASA Conf. Publication 2053.
Wood J. A. (1978b) Pallasites and the growth of parent meteorite planets (abstract). *Lunar Planet. Sci.* **9**, 1273–1275.
Wood J. A. (1981) On the nature of the pallasite parent body: Midcourse corrections (abstract). *Lunar Planet. Sci.* **12**, 1200–1202.
Yanai K. and Kojima H. (1995) Yamato-8451: A newly identified pyroxene-bearing pallasite. *Proc. NIPR Symp. Antarct. Met.* **8**, 1–10.

APPENDIX

A.1. Classificational Notes

A.1.1. Brenham-Marburg

At ≈70 μg/g, the Ge contents of Brenham and Marburg are the highest among main-group members. The remarkable similarity in composition and structure (rounded olivine) between Marburg and Brenham indicates a close relationship. As described by Buseck et al. (1967), the Marburg pallasite was recognized before 1965 by H.H. Nininger in a collection of unclassified minerals at the University at Marburg/Lahn, Germany. The origin of the original material is obscure; inquiries by Ramdohr (1965) indicated that it was supposedly found along a walkway near the Lahn river in 1906. The main mass is lost. We are confident that it is a Brenham sample, but A. El Goresy (personal communication, 1995) disputes this conclusion.

A.1.2. Phillips County

Scott (1977a) noted that Phillips County has a unique structure in which troilite is more abundant than metal. The olivine is in an FeS rather than an Fe-Ni matrix. The olivine composition in Phillips County is Fa18; among the main-group pallasites, only Zaisho (Fa18.3) is higher. Scott (1977a) analyzed a piece of Phillips County from the UCLA Meteorite Collection. We analyzed a specimen from the ASU collection; the O-isotope data of Clayton and Mayeda (1996) were determined on the olivine from the same piece.

To our surprise the Ir content in the ASU Phillips County sample was found to be 5 μg/g, the second highest in a PMG; that found by Scott (1977a) was 0.14 μg/g, one of the lowest in the PMG. The difference cannot be attributed differences in taenite content associated with selective etching of kamacite, since the new, high-Ir sample has a relatively low Ni content.

Our sample consisted of 3 pieces (because the metal abundance is low, the largest separable pieces are small); we hypothesized that one was a contaminant fragment of another, high-Ir meteorite. To check this we carried out independent counts of the ^{182}Ir 316-keV gamma in these samples. Within experimental error their Ir concentrations were found to be the same.

We then hypothesized that the ASU sample was mislabeled. However, a polished section showed it to have the same troilite-rich structure figured in Scott (1977a). Our next thought was that the UCLA specimen was mislabeled, but it shows the same troilite-rich texture. In the UCLA thick section collection is a grain mount whose label indicates that it contains olivine from the UCLA specimen (analyzed by Scott) as well as from the Field Museum of Natural History (FMNH). We analyzed a UCLA grain, a FMNH grain, and the olivine in the ASU specimen. Within error their compositions were all Fa18. Since there are only three pallasites with olivine in the Fa17-Fa19 compositional range, it appears that all of these samples must be Phillips County. We are forced to conclude that there is high degree of heterogeneity in Phillips County metal samples and their inclusions. As discussed in the text, there is evidence of rapid mixing and quenching during the formation of the PMG.